iScience

CellPress
OPEN ACCESS

Article

On-site detection and differentiation of African swine fever virus variants using an orthogonal CRISPR-Cas12b/Cas13a-based assay

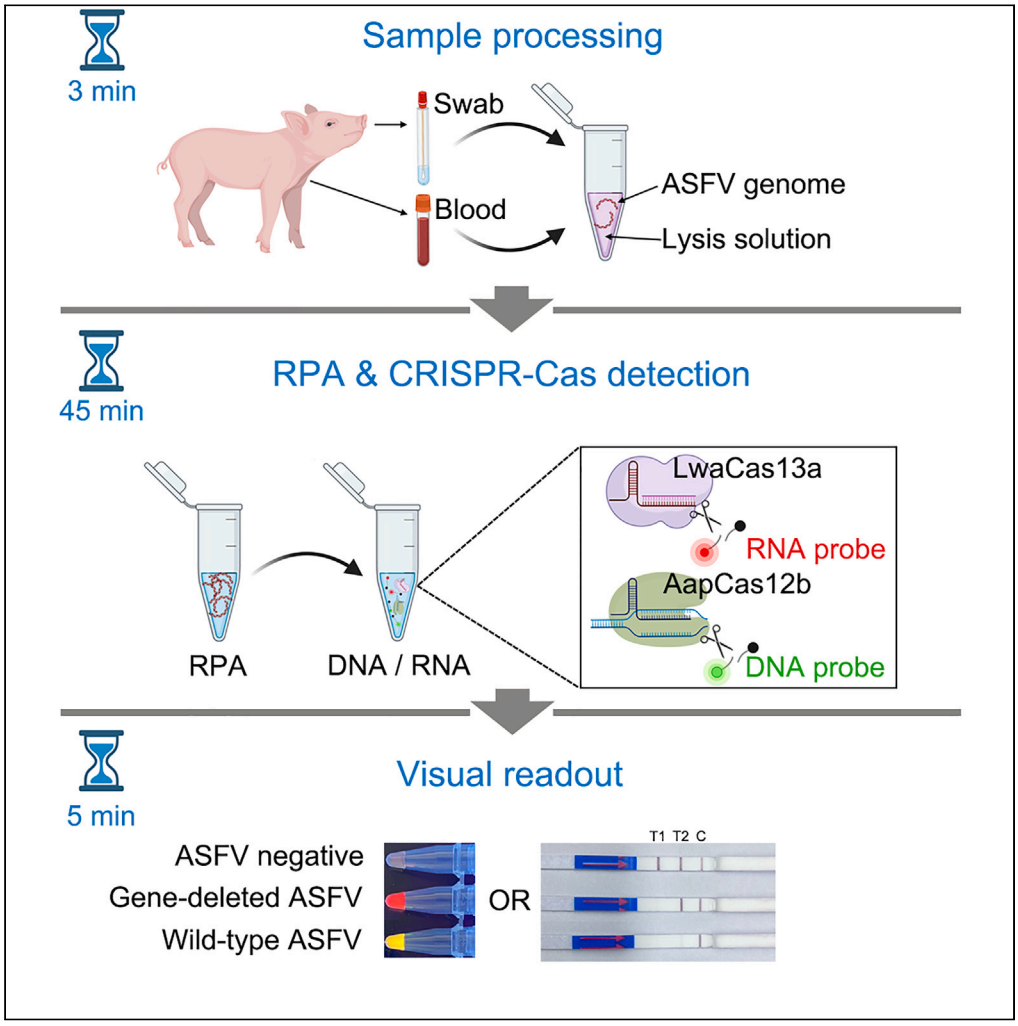

Zhe Wang, Yu Wang, Ying Zhang, ..., Yanfang Wang, Gaiping Zhang, Jianguo Zhao

wangyanfang@caas.cn (Y.W.)
zhanggaip@126.com (G.Z.)
zhaojg@ioz.ac.cn (J.Z.)

Highlights

On-site detection of ASFV and its variants in less than 60 min

An SNP is leveraged to differentiate between genotype I and II ASFVs

Equipment-free readout using a multiplexed lateral-flow strip

The assay detects ASFV in clinical samples with 100% sensitivity and specificity

Wang et al., iScience 27, 109050
April 19, 2024 © 2024
https://doi.org/10.1016/j.isci.2024.109050

iScience

CellPress
OPEN ACCESS

Article

On-site detection and differentiation of African swine fever virus variants using an orthogonal CRISPR-Cas12b/Cas13a-based assay

Zhe Wang,[1,2,3] Yu Wang,[4,5] Ying Zhang,[4,6,7] Guosong Qin,[4,6,7] Wenbo Sun,[8] Aiping Wang,[1,2,3] Yanfang Wang,[9,*] Gaiping Zhang,[1,2,3,10,*] and Jianguo Zhao[4,5,6,7,11,*]

SUMMARY

The African swine fever virus (ASFV) and its variants have induced substantial economic losses in China, prompting a critical need for efficient detection methods. Several PCR-based methods have been developed to discriminate between wild-type ASFV and gene-deleted variants. However, the requirement for sophisticated equipment and skilled operators limits their use in field settings. Here, we developed a CRISPR-Cas12b/Cas13a-based detection assay that can identify ASFV variants with minimal equipment requirements and a short turnaround time. The assay utilizes the distinct DNA/RNA collateral cleavage preferences of Cas12b/Cas13a to detect two amplified targets from multiplex recombinase polymerase amplification (RPA) in a single tube, and the results can be visualized through fluorescent or lateral-flow readouts. When tested with clinical samples in field settings, our assay successfully detected all ASFV-positive samples in less than 60 min. This assay provides a rapid on-site surveillance tool for detecting ASFV and its emerging variants.

INTRODUCTION

African swine fever (ASF) is a highly contagious, acute, lethal viral disease of domestic pigs and wild boars.[1] The World Organization for Animal Health (WOAH) lists ASF as a notifiable animal disease due to the high mortality it causes, its efficient transmissibility, and the serious socioeconomic impact it produces on food security and the international trade of pork and pork products.[2] China, the largest global pig producer that holds more than half of the world's domestic pig population, lost 40% of their pigs within one year as a result of high mortality of ASF and mandatory culling of the infected pigs; as a consequence, the price of pork doubled and even tripled over a long period of time after the first ASF outbreak in 2018.[3]Unfortunately, there is currently no commercially available vaccine or drug for ASF, which means that control measures primarily rely on the early diagnosis and culling of infected animals.[4]

African swine fever virus (ASFV) is the causative agent of ASF, belonging to the genus *Asfivirus* within the family *Asfarviridae*. The ASFV virion has a complex multilayered architecture[5] and a large double-stranded DNA genome of 170–193 kbp that contains 150–167 open reading frames (ORFs) depending on the virus isolate.[6] Among these genes, *B646L*, which encodes the major capsid protein p72, is highly conserved within each genotype of ASFV.[7] Therefore, most validated and commonly used polymerase chain reaction (PCR)-based diagnosis methods target *B646L*. Recently, *G1211R*, the DNA polymerase gene of ASFV, was also used as a target for field-deployable, sensitive ASFV detection.[8] Thorough investigations have been undertaken for virulence-associated genes, such as *EP402R* (encoding the ASFV hemagglutinin) and multigene family (*MGF*) *360-505R* (host type I interferon inhibitors, including *MGF505-2R*) because they were found to be missing in naturally attenuated ASFV isolates, which can confer up to 100% protection against homologous viral challenge.[9–12] Based on these findings, several studies deleted one or more of these virulence factors from different ASFVs to construct gene-deleted live attenuated vaccine candidates with promise.[3,13–19]

[1]School of Life Sciences, Zhengzhou University, Zhengzhou 450001, China
[2]Longhu Laboratory, Zhengzhou 450046, China
[3]Henan Key Laboratory of Immunobiology, Zhengzhou 450001, China
[4]Key Laboratory of Organ Regeneration and Reconstruction, Institute of Zoology, Chinese Academy of Science, Beijing 100101, China
[5]Savaid Medical School, University of Chinese Academy of Sciences, Beijing 100049, China
[6]Beijing Institute for Stem Cell and Regenerative Medicine, Beijing 100101, China
[7]Institute for Stem Cell and Regeneration, Chinese Academy of Sciences, Beijing 100101, China
[8]Shandong Key Laboratory of Animal Disease Control and Breeding, Institute of Animal Science and Veterinary Medicine, Shandong Academy of Agricultural Sciences, Jinan 250100, China
[9]State Key Laboratory of Animal Nutrition, Institute of Animal Science, Chinese Academy of Agricultural Sciences, Beijing 100193, China
[10]School of Advanced Agricultural Sciences, Peking University, Beijing 100871, China
[11]Lead contact
*Correspondence: wangyanfang@caas.cn (Y.W.), zhanggaip@126.com (G.Z.), zhaojg@ioz.ac.cn (J.Z.)
https://doi.org/10.1016/j.isci.2024.109050

Based on the 3′ end sequences of the *B646L* gene, ASFVs can be classified into 24 genotypes, most of which have been confined to Africa, except for genotype I and genotype II strains.[20] The first introduction of genotype I ASFV outside of Africa was to Portugal in 1957 and spread from there to other European countries. After 30 years, most affected countries eradicated genotype I ASFV by the mid-1990s, except for Italy Sardinia.[21] In 2007, genotype II ASFV entered Georgia from the east coast of Africa and later spread quickly to other neighboring countries and the European Union.[22] In August 2018, Georigia-07-like genotype II ASFV emerged in China, which represented the first occurrence of ASF in Asia.[23] Since then, this highly lethal Georigia-07-like genotype II ASFV (termed wild-type ASFV) rapidly spread to most provinces in China within a short time and has become the dominant strain circulating until now.[24,25] These wild-type ASFVs cause typical acute clinical signs, including high fever, depression, skin redness, and respiratory distress, with nearly 100% mortality.[26,27]

In 2021, two low virulent genotype I ASFVs were isolated from domestic pig farms in Shandong and Henan Provinces in China.[28] Compared to the whole genomes of virulent genotype I ASFV, low virulent genotype I ASFV deleted 10 ORFs (*MGF110-11L*, *MGF110-12L*, *MGF360-6L*, *MGF360-10L*, *MGF360-11L*, *MGF360-12L*, *MGF360-13L*, *MGF360-14L*, *MGF505-1R*, and *MGF505-2R*) and had 5 truncated ORFs (*EP402R*, *EP153R*, *MGF360-9L*, *MGF505-3R*, and *MGF100-2L*). Animal challenge experiments showed that low virulent genotype I ASFV strains have a prolonged incubation period and cause chronic disease but efficient transmissibility in pigs. Infected pigs developed low-level viremia but shed viruses continuously via oral and rectal routes to swine herds, which makes early diagnosis and timely implementation of stringent control measures more challenging. Most recently, *MGF505-2R* gene-deleted ASFV emerged in Guangxi Province, Southern China, in 2022.[29,30] Given that *MGF505-2R* is a virulence-related gene[14] and that both genotype I and II ASFV strains with *MGF505-2R* deletion are attenuated,[3,28] and it is reasonable to assume that these newly identified gene-deleted field isolates may be less virulent and cause asymptomatic transmission like other low virulent ASFV variants.[9,10,28] Moreover, we cannot fully exclude the possibility that reassortment among genotype I virus, genotype II virulent virus, and genotype II attenuated virus may occur when a pig is infected with different ASFVs simultaneously.[28] Unfortunately, this hypothesis was very recently confirmed by Zhao et al., who report three recombinants of genotype I and II ASFVs in pigs in China.[31] Therefore, in routine ASFV surveillance, it is crucial not only to detect the presence of ASFV but also to identify their molecular characteristics.

Considering the aforementioned facts, triplex real-time PCR targeting *MGF505-2R* and other conserved genes has been proposed and evaluated on clinical samples for the differentiation of *MGF505-2R* gene-deleted ASFV from wild-type ASFV.[29,32] Later, several groups also developed PCR-based assays to differentiate low virulent genotype I from wild-type genotype II strains.[4,24,33–35] However, PCR-based methods are usually conducted in central laboratories by highly skilled operators and require expensive instruments, making them less suitable for field applications.[36] Isothermal nucleic acid amplification (INA), such as recombinase polymerase amplification (RPA)[37,38] and loop-mediated isothermal amplification (LAMP),[39] circumvents the use of thermal cyclers and is usually faster than real-time PCR, but it has the disadvantages of nonspecific amplification and low sensitivity.[40] Therefore, an assay that combines the ease of use of INA with the accuracy of real-time PCR is urgently needed for ASFV surveillance in the field.

Clustered regularly interspaced short palindromic repeats-based diagnostics (CRISPR-Dx) are promising technologies to fulfill these unmet needs. CRISPR systems are key components of the adaptive immune system in bacteria and archaea.[41] In addition to broad use as genome engineering tools, CRISPR-associated (Cas) enzymes were repurposed to improve the specificity and sensitivity of INA.[42,43] The Cas enzyme recognizes and cleaves specific INA products (namely, *cis*-cleavage) that contain sequences complementary to the CRISPR RNA (crRNA). Relying on this strict variation inspection mechanism, INA eliminates the interference from primer oligomers or nonspecific amplicons through coupling with the CRISRP-Cas system.[40,44] After activation by the target sequence, the Cas enzyme acquires collateral cleavage activity to nonspecific nucleic acids (namely, *trans*-cleavage), which converts single-turnover *cis*-cleavage activity to multi-turnover *trans*-cleavage activity.[45] Engagement of this signal amplification mechanism (up to 10,000-fold) increases the sensitivity of INA to a single molecule range.[46]

According to the number of targets detected in a single reaction, CRISPR-Dx can be classified into two types: single target detection and multiple target detection. Although some studies have developed sensitive and field-deployable CRISPR-Dx, most of them are constrained to single target detection.[8,46–49] Notably, multiplex CRISPR-Dx is urgently needed in a wide range of circumstances, such as target gene degradation, gene copy variation, amplification errors, and virus mutation.[50] Moreover, multiplex CRISPR-Dx will provide more information to improve detection accuracy and efficiency and reduce the cost per target.[41] A previous study reported a multiplex nucleic acid detection platform that can detect four different target genes in a single test tube by taking advantage of the orthogonal *trans*-cleavage base preferences of four Cas enzymes (LwaCas13a, PsmCas13b, CcaCas13b, and AsCas12a).[51] Considering the signal leakage caused by the lack of absolute orthogonal *trans*-cleavage activity, Tian et al. simplified the four-gene detection system to a dual-gene detection platform based on LbCas12a and LbuCas13a, which orthogonally cleave ssDNA and ssRNA fluorescent reporters, respectively. In addition, by integration with custom-built fluorescence readout equipment, a portable CRISPR-Dx platform was developed for field application.[50] To eliminate the need for fluorescence instruments and achieve better point-of-care test (POCT) feasibility, the lateral flow strip was introduced to CRISPR-Dx for colorimetric readout.[44] However, such approaches have failed to address the inefficient cleavage activity of Cas12a in orthogonal Cas12a/Cas13a detection assays, even after optimizing some key factors.[50] Low enzyme activity may lead to false-negative results and prolonged reaction time, especially using lateral flow strip readout.[44]

Lateral flow strip technology offers a straightforward visualization of the collateral cleavage activity inherent to many CRISPR-based diagnostics. It eliminates the reliance on fluorescence-detection devices and provides a simple and accessible means of detecting ASFV variants in the field. However, it is important to note that the commonly used lateral flow strip (Millenia 1T, Germany) was not initially designed specifically for CRISPR-based diagnostics. As a result, when there is a high target concentration in the sample, it can sometimes lead to an invisible control band on the strip. This can make it challenging to differentiate between positive results and invalid lateral flow tests.

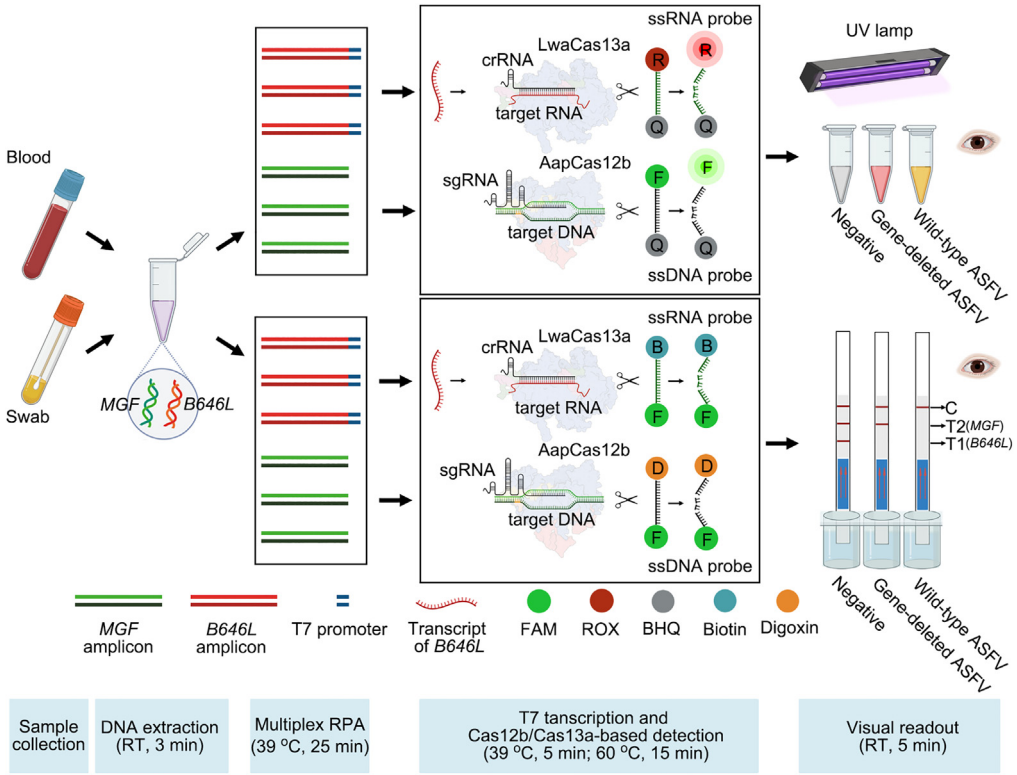

Figure 1. Schematic illustration of OBServe

The ASFV genome was extracted from swine blood or swab samples at room temperature (RT) in 3 min. Two target genes, *B646L* and *MGF505-2R (MGF* for short), were amplified in a multiplex RPA reaction using the T7 promotor-tagged primer set and conventional primer set, respectively. The amplified *B646L* gene is T7-transcribed into RNA, and binding to the crRNA (CRISPR RNA) activates Cas13a and triggers collateral cleavage of quenched fluorescent ssRNA probes or FAM/biotin-labeled ssRNA probes. Cas12b is guided to *MGF* amplicons by a single guide RNA (sgRNA), triggering collateral cleavage of quenched fluorescent ssDNA probes or digoxin/biotin-labeled ssDNA probes. Detection results can be visualized using a portable ultraviolet (UV) lamp (302 nm) for fluorescence readout and a lateral flow strip for instrument-free detection. In all Figure legends, "F" in the circle is short for FAM, "R" in the circle is short for ROX, "Q" in the circle is short for quencher, "B" in the circle is short for biotin, and "D" in the circle is short for digoxin.

In this work, we developed OBServe (orthogonal CRISPR-Cas12b/Cas13a-based dual-gene detection assay that served as a field-deployable tool) for the rapid detection of ASFV and its variants in the field settings. We systematically optimized the multiplex RPA reaction to achieve a balanced amplification efficiency. By addressing the incompatibility between Cas12 and Cas13 assays, we successfully generated balanced signals in two independent detection channels. In addition, we designed a multiplexed lateral flow assay that enables visual colorimetric readout without the need for specialized equipment. We demonstrated that OBServe can detect ASFV and its variants in field samples with 100% sensitivity and specificity compared to real-time PCR in less than 60 min. Moreover, we design and validate the OBServe assay to discriminate between genotype I and II ASFV variants based on a single-nucleotide difference. OBServe represents a rapid and sensitive diagnostic technology for monitoring ASFV and its variants in the field settings.

RESULTS

Working principle of OBServe

OBServe can be divided into four sequential steps, including sample collection and preparation, multiplex RPA preamplification, orthogonal CRISPR-Cas12b/Cas13a detection, and fluorescence or lateral flow readout (Figure 1).

We first collected inactivated swine blood or swab samples from our collaborator and stored them in a −80°C refrigerator until ready for use. To eliminate the time-consuming column- or bead-based nucleic acid extraction process, we introduced a commercially available fast DNA extraction solution (Zhongdao Biotech, China) that works at ambient temperature and is completed in 3 min and was initially designed for real-time PCR. Our results indicated that this simple extraction method was compatible with downstream preamplification and CRISPR-Cas detection (data not shown).

For multiplex RPA, we designed two pairs of primers targeting the genes *B646L* and *MGF505-2R* ("*MGF*" for short). Notably, *B646L* was chosen for sensing the presence of ASFV because it is highly conserved and indispensable for virus morphogenesis. Moreover, to ensure the high sensitivity of detection, we appended the T7 RNA polymerase promoter to the 5′ end of the forward primer of *B646L* to allow for

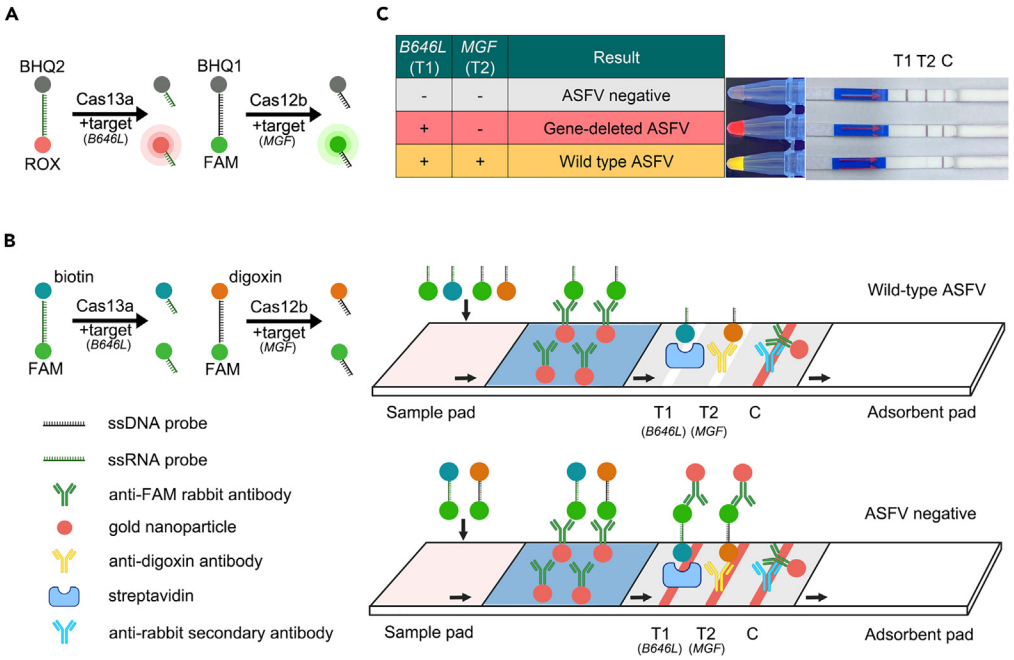

Figure 2. Signal readout and interpretation of OBServe

(A) Schematic diagram of fluorescence readout.

(B) Schematic diagram of lateral flow readout.

(C) Detection result interpretation.

transcription, which is a well-known signal amplification process. *MGF* was amplified by conventional RPA primer sets and used to differentiate between wild-type and *MGF* gene-deleted ASFVs.

In the orthogonal CRISPR-Cas12b/Cas13a detection system, the Cas enzyme recognizes specific RPA amplicons that have a complementary sequence to the guide RNA, thereby eliminating interference from nonspecific amplicons and primer oligomers. Then, the activated Cas enzyme converts the filtered RPA signal to a fluorescent color or a line on the lateral flow strip via collateral cleavage of single-strand DNA (ssDNA) or single-strand RNA (ssRNA) probes. Multiplex CRISPR-based detection builds on the orthogonal collateral cleavage preferences of Cas orthologs. Cas13a, a crRNA guide RNase, binds *B646L* transcripts generated via *in vitro* transcription from T7 promoter-tagged DNA amplicons, triggering collateral cleavage of ssRNA probes but not ssDNA probes. In contrast, Cas12b, a single guide RNA (sgRNA) guides DNase, recognizes *MGF* DNA amplicons directly, and exhibits orthogonal collateral cleavage against ssDNA probes but not ssRNA probes.

To facilitate in-tube fluorescence readout, 5′-ROX-UUUUUU-BHQ2-3′ ssRNA probes and 5′-FAM-TTTTTT-BHQ1-3′ ssDNA probes were designed for Cas13a and Cas12b, respectively (carboxy fluorescein, FAM; carboxy-X-rhodamine, ROX; black hole quencher 1/2, BHQ1/2). When the fluorescent probes are intact, BHQ quenches the fluorescence emitted from FAM or ROX through fluorescence resonance energy transfer (FRET). However, degraded fluorescent probes separate the fluorophore from the quencher, resulting in red fluorescence that indicates the collateral cleavage activity of Cas13a triggered by *B646L* or green fluorescence representing *MGF*-activated Cas12b (Figure 2A). Colored fluorescence can be read by the naked eye under ultraviolet (UV) light (302 nm) with a UV safety shield. In the absence of both target genes, OBServe showed no fluorescence, indicating that no ASFV was detected. When *MGF* gene-deleted ASFV is sensed, OBServe emits red fluorescence. In the presence of wild-type ASFV, OBServe shows bright yellow fluorescence, derived from the overlapping of green and red fluorescence (Figure 2C).

Lateral flow readout was achieved using a commercially available lateral flow strip (HybriDetect 2T, Milenia) that is designed to simultaneously detect two different analytes. This test strip consists of a sample pad (embedded with gold nanoparticle-labeled anti-FAM rabbit antibodies), test band 1 (T1, coated with streptavidin), test band 2 (T2, coated with anti-digoxin antibodies), control band (C, coated with anti-rabbit secondary antibodies), and adsorbent pad (Figure 2B). Initially, HybriDetect 2T was developed for the simultaneous detection of two different analytes labeled with FAM, biotin, and digoxin. To employ this simple visualization technique, we designed new ssRNA probes flanked by FAM and biotin at separate ends and a short ssDNA probe with FAM at one end and digoxin at the other. After the orthogonal CRISPR-Cas12b/Cas13a reaction, we deposited the product on the sample pad area of the test strip, at which point both ssRNA and ssDNA probes were labeled with gold nanoparticles (Au NPs) via the binding of FAM to anti-FAM antibodies. Capillary forces cause these gold complexes to diffuse to T1 at first, where streptavidin specifically binds the biotin end of ssRNA probes and forms a visible dark purple band when the ssRNA probes are intact. However, when ssRNA probes are cleaved because of the presence of the target gene *B646L* and the collateral activity of Cas13a, Au NP-labeled antibodies separate from the biotin molecules, leading to invisible T1 that indicates the presence

of ASFV. For T2, *MGF* detection with Cas12b is almost identical to *B646L*, except for the replacement of streptavidin/biotin interaction within high affinity between digoxin and digoxin-specific antibodies. The presence of wild-type ASFV is responsible for the invisible T2. In contrast, detection of *MGF* gene-deleted ASFV led to a clear visible color on T2 but disappeared on T1. Uncaptured Au NPs travel further to the control band and are fixed there, creating a dark purple color and validating this test. The adsorbent pad facilitates liquid flow across the strip, as indicated by the black arrow (Figure 2C).

Development of multiplex RPA of the ASFV *B646L* and *MGF* genes

To monitor most subtypes of ASFV, we targeted the highly conserved regions of the *B646L* and *MGF* genes according to the multiple nucleotide sequence alignment of 27 no-redundant ASFV genomes[52] (Figure 3A; Figure S1). We designed and tested 92 sets of primers for the *B646L* gene and 48 sets of primers targeting the *MGF* gene according to the manufacturer's primer design guidance (Figure S2). We assessed the performance of these primers using a classical fluorophore quencher-labeled reporter assay[43,53] (Figure 2A) based on Cas13a or Cas12b and chose the best-performing primer set of each target for the compatibility test.

In this test, we found that the efficiency of the *MGF* primer set was inversely proportional to the concentration of the *B646L* primer set (Figure 3B). To eliminate this inhibitory effect, we initially incorporated six sets of primers targeting different regions of *MGF* into the multiplex RPA reaction, but all of them were inhibited by the *B646L* primer set (Figure 3C). We then wondered which primer in the *B646L* primer set caused this inhibitory effect. By adding either forward primer or reverse primer to the single-plex RPA reaction targeting *MGF*, we noticed that the T7-tagged forward primer was mainly responsible for the inhibitory effect (Figure 3D). Therefore, we changed the nucleotide sequence of the forward primer of *B646L* but found that this strategy had no effect on improving the efficiency of the *MGF* primer set (Figure 3E). We next gradually lowered the concentration of the *B646L* primer set in the multiplex RPA reaction and found that the efficiency of the *MGF* primer set was restored (Figure 3F). Therefore, we selected primer F2 of *B646L* for further experiments and determined that the upper limit concentration of F2 was 125 nM. To achieve balanced amplification efficiency for the two targets, we adjusted the primer ratio of *B646L* and *MGF* to 1:3 (Figure 3G). Finally, we titrated the concentration of primers to determine 62.5 nM *B646L* primer set combined with 200 nM *MGF* primer set as the optimal primer concentration for multiplex RPA (Figure 3H). In addition, we optimized the concentration of magnesium, temperature, and reaction time in the multiplex RPA reaction (Figure S3).

Establishment of the orthogonal CRISPR-Cas12b/Cas13a detection platform

AapCas12b is a newly identified Cas enzyme from *Alicyclobacillus acidiphilus* with collateral cleavage activity against nonspecific ssDNA molecules upon target DNA recognition. Compared with previously reported LbCas12a, AapCas12b processes its nuclease activity over a wide range of temperatures and requires simper protospacer adjacent motif (PAM) sequences (5′-TTTN-3′ for LbCas12a versus 5′-TTN-3′ for AapCas12b),[54] which allows for more flexibility in reaction condition optimization and a broader target range for primer design when coupled with preamplification. These attractive features make AapCas12b more suitable for viral nucleic acid sensing since the viral genome is prone to mutate during replication.

Previous studies reported a portable detection platform based on the orthogonal CRISPR-Cas12a/Cas13a system.[44,50] In this technique, the efficiency of Cas12a is suppressed by Cas13a assay components (T7 RNA polymerase, rNTPs, Cas13a enzyme, and crRNA), leading to lower fluorescence[50] or a weaker test band on lateral flow strips for Cas12a detection compared with Cas13a.[44] Our initial consideration to address the aforementioned issues was introducing a thermophilic Cas12 ortholog, for example, AapCas12b, into the orthogonal CRISPR-Cas12/Cas13 system. In the orthogonal CRISPR-Cas12b/Cas13a system, the reaction temperature was first set at 37°C for Cas13a detection, followed by heating to 60°C, when Cas13a assay components are inactivated[55] but Cas12b works with higher efficiency.[56] In this design, Cas13a and Cas12b work independently at different stages of the reaction.

We first purified the LwaCas13a, LbCas12a, and AapCas12b proteins from the prokaryotic expression system (Figure S4). Next, we assessed the *cis*-cleavage activity of LwaCas13a on the ssRNA target and AapCas12b on the dsDNA target (Figure S5A), together with orthogonal collateral *trans*-cleavage preferences on ssDNA or ssRNA fluorescent probes (Figure S5B). After validating the feasibility of the orthogonal CRISPR-Cas12b/Cas13a reaction, we performed the CRISPR-Cas12a/Cas13a reaction and CRISPR-Cas12b/Cas13a reaction in parallel. We found that at 37°C, the efficiencies of Cas12a and Cas12b were both inhibited. However, at 60°C, the efficiency of Cas12b was restored, generating a strong fluorescent signal in a short time, comparable to that of the Cas13a detection assay (Figure 4A; Figure S6A). However, Cas12 assay components did not interfere with the activity of Cas13a in different orthogonal CRISPR-Cas12/Cas13 systems (Figure S6B).

Guide RNA is an important determinant for the kinetics of the Cas enzyme in CRISPR-Dx. We designed 14 guide RNAs targeting different regions of the RPA amplicon amplified by the primers used for the *B646L* gene and *MGF* gene. We screened these guide RNAs using a multiplex RPA product in a fluorophore quencher-labeled reporter assay and found that *MGF*-targeted sgRNA-2 and *B646L*-targeted crRNA-5 outperformed other guide RNAs in terms of raw fluorescence intensity or fluorescence fold change at the endpoint of the reaction (Figure 4B; Figure S7). Therefore, sgRNA-2 and crRNA-5 were selected to develop the orthogonal CRISPR-Cas12b/Cas13a detection assay.

According to a previous study,[50] we next optimized the reaction buffer and concentration of rNTPs. We confirmed NEBuffer 1.1 as the optimal reaction buffer, and 0.25 mM rNTPs were beneficial for a more balanced detection signal (Figures 4C and 4D). Another study reported that the viscous RPA reaction composition interferes with downstream Cas13a-based target detection. However, the activation of the Cas enzyme is quantitative with respect to the nucleic acid target abundance in the CRISPR-Cas-based detection assay.[46] Therefore, we titrated the RPA product input ratio of the orthogonal CRISPR-Cas12b/Cas13a detection assay to weigh the pros and cons. An input of 25% (v/v) RPA products in OBServe generated the most balanced detection signals (Figure 4E).

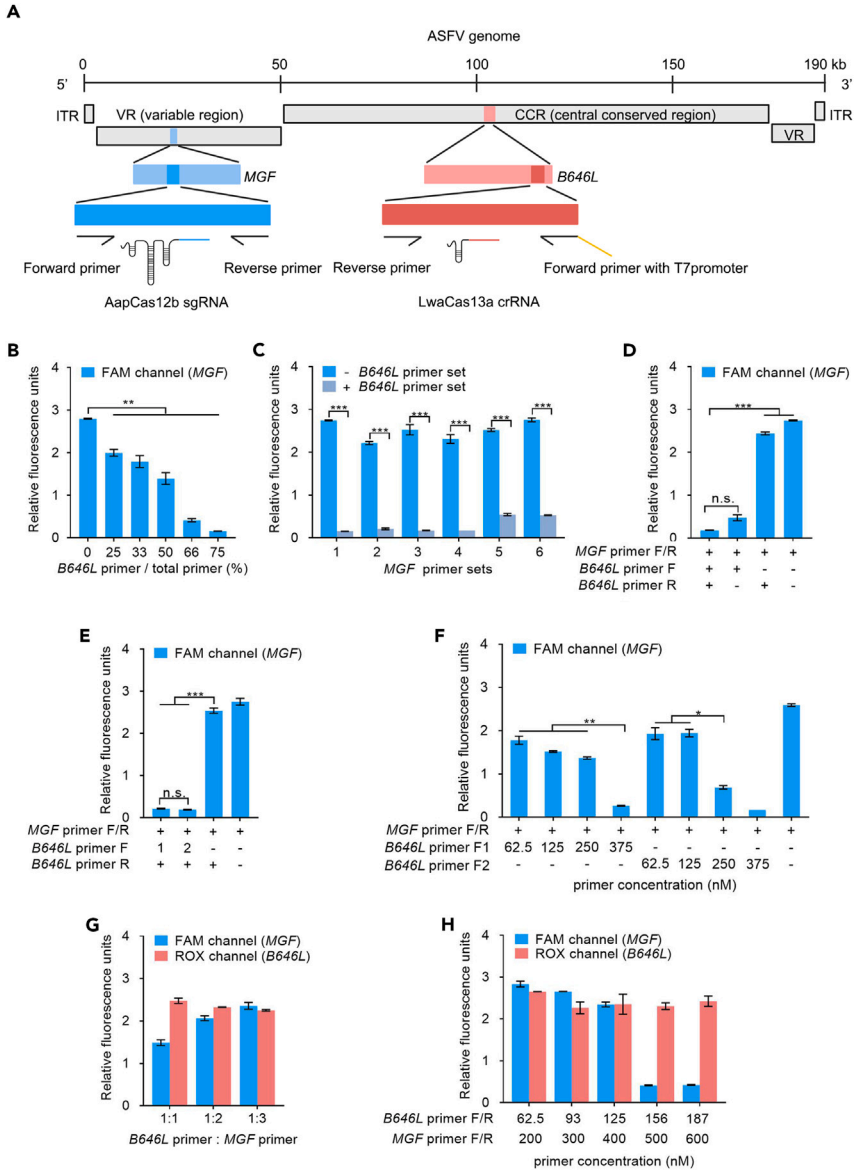

Figure 3. Development and optimization of the multiplex RPA reaction

(A) Genome map of ASFV showing gene targets, RPA primers, and guide RNAs. *B646L* forward primer flanking with T7 promoter sequence at the 5′ terminal for *in vitro* transcription (see also Figures S1 and S2). ITR: inverted terminal repeat, VR: variable region, CCR: central conserved region.

(B) Impact of different ratios of the *B646L* primer set on *MGF* amplification efficiency. After multiplex RPA, products were added into the orthogonal Cas12b/Cas13a detection system to assess amplification efficiency using the endpoint fluorescence signal, *MGF* in the FAM channel, and *B646L* in the ROX channel. The total primer concentration was maintained at 2,000 nM.

(C) Comparison of the amplification efficiency of six sets of *MGF* primers in the presence or absence of the *B646L* primer set.

(D) Identification of the cause of *MGF* amplification inhibition. F: forward primer, R: reverse primer.

(E) Comparison of *MGF* amplification efficiency using different *B646L* forward primers.

(F) Titration of *B646L* forward primer concentration for *MGF* amplification efficiency.

(G) Adjustment of the ratios of the *B646L* primer set *and MGF* primer set. The concentration of *B646L* primer F1/R was maintained at 125 nM, and 125, 250, and 375 nM *MGF* primer F/R was used.

(H) Fine-tune the concentration of primer sets to balance dual-gene amplification.Data are represented as mean ± SEM (standard error of the mean), n = 2. Unpaired Student's t test (two-tailed) was used to determine the significant differences; *, $p < 0.05$; **, $p < 0.01$; ***, $p < 0.001$, n.s., not significant.

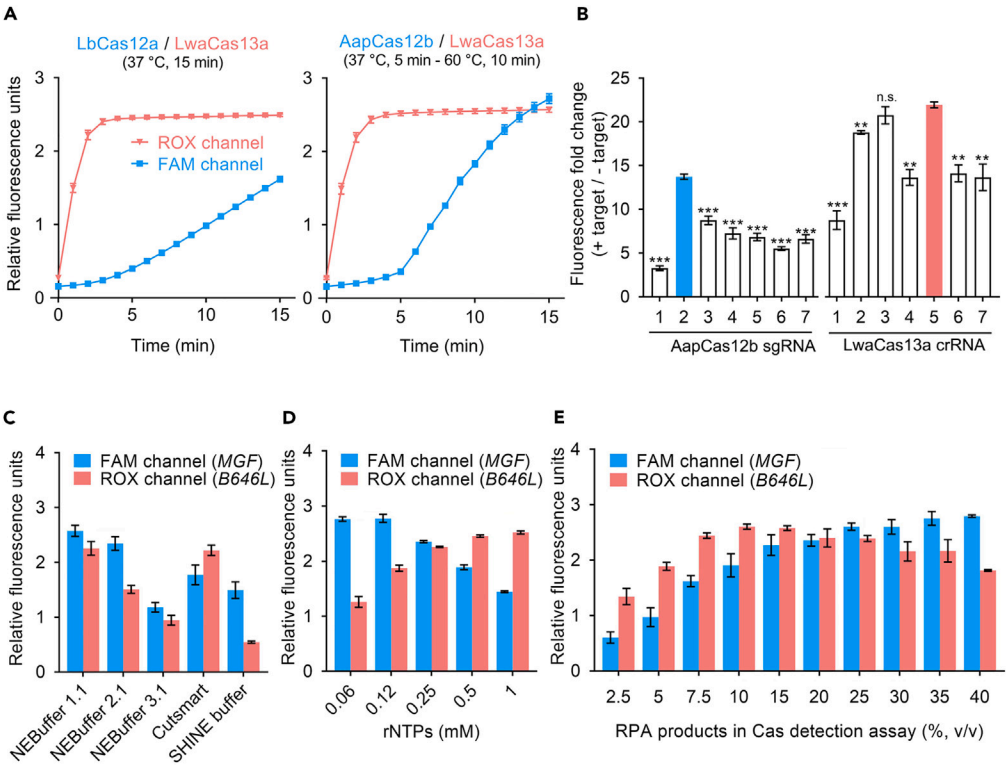

Figure 4. Establishment and optimization of the orthogonal Cas12b/Cas13a detection assay

(A) Comparison of the performance of the orthogonal Cas12/Cas13 detection assay using either LbCas12a or AapCas12b (see also Figures S4–S6).

(B) Fluorescence fold change using different single guide RNAs (sgRNA) in AapCas12b detection assay or crRNA (CRISPR RNA) in LwaCas13a detection system when incubated with RPA amplified target or no template control. For AapCas12b (activated by *MGF* RPA products), the assay was performed at 60°C, and collateral activity was measured after 10 min by endpoint fluorescence. For LwaCas13a (activated by *B646L* RPA products), the assay was performed at 37°C, and endpoint fluorescence was recorded at 5 min (see also Figure S7).

(C) Comparison of different reaction buffers for effects on the performance of the orthogonal Cas12b/Cas13 detection assay.

(D) Comparison of the effects of different concentrations of rNTPs on the performance of the orthogonal Cas12b/Cas13 detection assay.

(E) Comparison of different ratios of RPA product input for effects on the performance of the orthogonal Cas12b/Cas13 detection assay. Data are represented as mean ± SEM (standard error of the mean), n = 3. Unpaired Student's t test (two-tailed) was used to determine the significant differences; *, $p < 0.05$; **, $p < 0.01$; ***, $p < 0.001$, n.s., not significant.

Evaluation and clinical validation of OBServe for ASFV detection

To determine the detection limit of OBServe in different detection channels, we conducted experiments using serially diluted plasmids (Figure S8A) carrying either one target gene or both target genes. Our data show that OBServe has a sensitivity of 8 copies/μL in different detection channels, using either fluorescence readout or lateral flow readout (Figure 5A), which is comparable to that of real-time PCR[32,57,58] (Figure S8B). Furthermore, two dilution series of ASFV-positive field samples were used to evaluate the limit of detection (LOD) of OBServe. The results revealed that OBServe achieved a sensitivity comparable to real-time PCR cycle thresholds (Ct) value of 36.65 (Figure S9).

To evaluate the clinical performance of OBServe, we conducted tests on a panel of 37 veterinary samples with Ct values ranging from 21.37 to 35.2. In this assessment, OBServe displayed a remarkable sensitivity and specificity of 100% in detecting ASFV (Figures 5B–5D). Notably, as shown in Figure 5B, our results and subsequent confirmation by real-time PCR indicated the presence of only one *MGF* gene-deleted ASFV in the veterinary samples. This suggests that wild-type ASFV remains the predominant strain in Henan Province, China.

After evaluating OBServe in the academic setting, we collected 17 field samples in a pig farm and then performed OBServe in the field setting to assess its feasibility for on-site detection. OBServe correctly identified all real-time PCR-positive samples in less than 60 min, while requiring minimal equipment (Figure S10).

To assess the potential for cross-reactivity with other swine pathogens, we tested 10 nucleic acid samples extracted from common swine pathogens, including viruses and bacteria. OBServe did not exhibit any cross-reactivity with these pathogens (Figure 5E).

Collectively, these findings demonstrate that OBServe exhibits excellent sensitivity and specificity in detecting and differentiating between wild-type and MGF gene-deleted ASFVs.

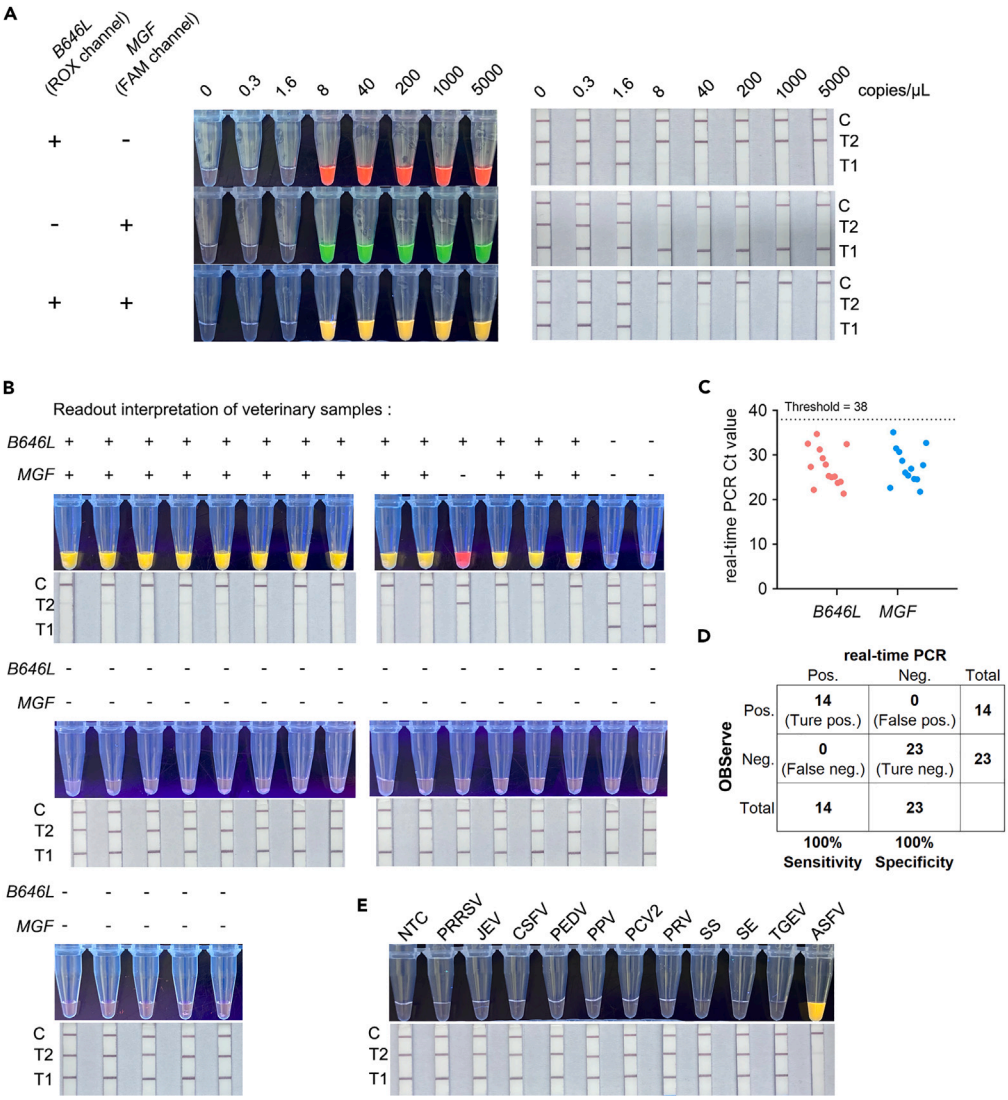

Figure 5. Evaluation of the performance of OBServe using synthetic gene templates and veterinary samples

(A) Sensitivity of OBServe in different detection channels using serial diluted plasmid containing synthetic gene fragment (see also Figure S8).

(B) Endpoint fluorescence or lateral flow readout of 37 veterinary samples.

(C) Ct values of 37 veterinary samples using a validated triplex real-time PCR kit (Lijian, China).

(D) Concordance table between real-time PCR and OBServe for 37 veterinary samples.

(E) Specificity of OBServe by examining ASFV and other common swine pathogens. Porcine reproductive and respiratory syndrome virus (PRRSV), Japanese encephalitis virus (JEV), classical swine fever virus (CSFV), porcine epidemic diarrhea virus (PEDV), porcine parvovirus (PPV), porcine circovirus type 2 (PCV2), pseudorabies virus (PRV), swine erysipelas (SE), swine salmonellosis (SS), and transmissible gastroenteritis virus (TGEV).

Differentiation of genotype I and II ASFVs using single-nucleotide specificity of OBServe

It has been reported that both genotype I[9,10,14] and II[3,13] ASFVs with *MGF* gene deletion are attenuated. Between them, low virulent genotype I ASFV attracts much attention because infected pigs show milder symptoms but spread viruses continuously to swine herds, which makes early disease diagnosis and control more difficult.[28] Although *MGF* gene-deleted genotype II ASFV has not been reported in China so far, it is important to monitor this variant, since it may cause similar problems as low virulent genotype I ASFV. Several real-time PCR have been developed for the differentiation of genotype I and II ASFVs,[24,33,34,59] but these methods are usually conducted in central laboratories by highly skilled technicians, which is unsuitable for on-site detection. Hence, a rapid, sensitive, and field-deployable genotyping method is desirable for ASFV variants surveillance.

A previous study has demonstrated that it is difficult to design desirable primers and probes that can differentiate genotype I from II ASFV based on the *B646L* gene due to high frequent repeat sequences and high AT content.[24] *G1211R*, which encodes the DNA polymerase gene

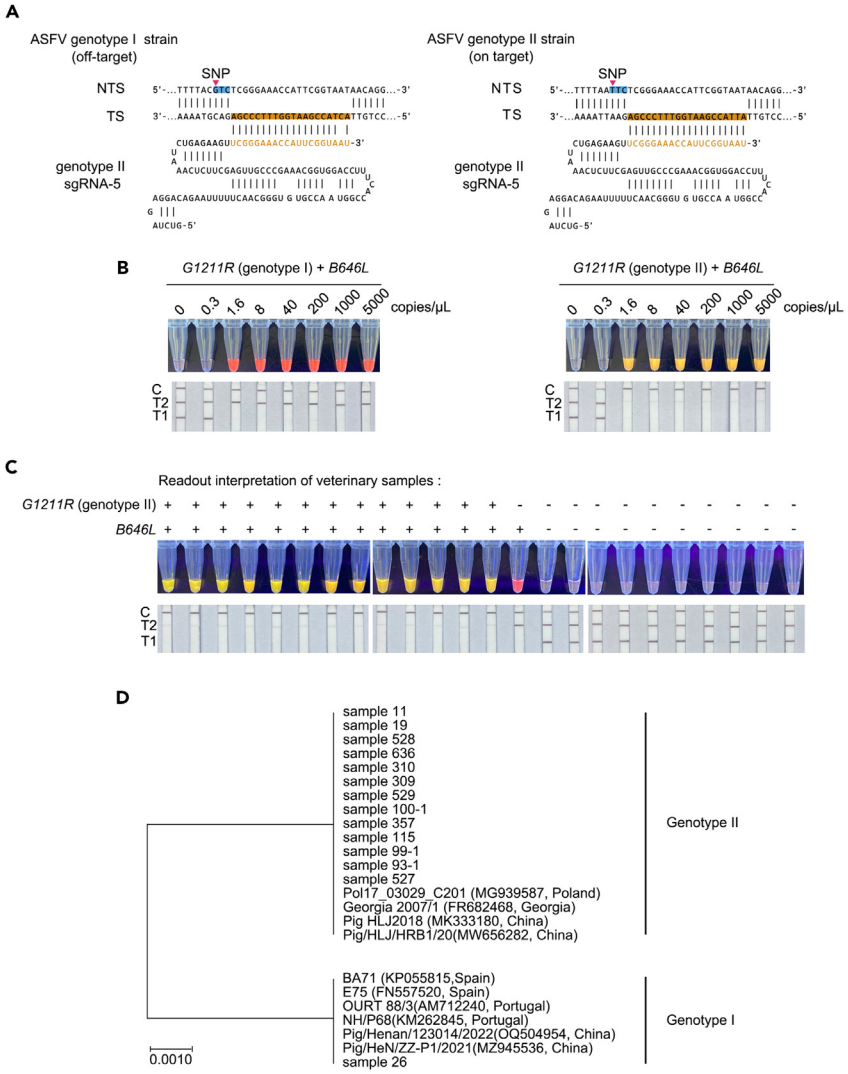

Figure 6. Discrimination of genotype I and II ASFV strains using OBServe

(A) Schematic of sgRNA design for sensing a single-nucleotide mismatch distinction between genotype I and II ASFV strains at the protospacer adjacent motif (PAM).

(B) Determination of the limit of detection (LOD) at different concentrations of plasmids containing synthetic gene fragments.

(C) Evaluation of the performance of OBServe for genotype I and II ASFV strains discrimination in veterinary samples.

(D) Phylogenetic analysis of 14 ASFV-positive veterinary samples based on partial sequences of the *B646L* gene. The maximum likelihood method was used to construct phylogenetic trees using MEGA X software. The phylogeny was inferred following 1,000 bootstrap replications. The scale bar indicates nucleotide substitutions per site.

of ASFV, is essential to ASFV life cycle[60,61] and highly conserved within each genotype of ASFV.[52] Most recently, this gene was used to develop a field-deployable, ultrasensitive, and accurate diagnostics of ASFV based on CRISPR-Cas system.[8] However, whether *G1211R* could be used to distinguish genotype I from II ASFV still needs to be explored.

In this section, we employed OBServe to differentiate genotype I and II ASFVs. The same strategy used in wild-type and *MGF* gene-deleted ASFVs discrimination was adopted here. Briefly, in the orthogonal CRISPR-Cas12b/Cas13a detection assay, we utilized the Cas13a reaction for the detection of the highly conserved *B646L* gene to capture all ASFV-positive samples and developed Cas12b-based detection of *G1211R*, which would allow differentiation between genotype I and II ASFVs by sensing a single-base-pair difference in the PAM sequence of Cas12b (Figure 6A). In the presence of genotype I ASFV, Cas12b stayed in an inactive state due to the lack of a perfectly matched PAM sequence, and only Cas13a was activated by *B646L* transcripts, triggering collateral activity to the ROX-labeled ssRNA reporter, resulting in red fluorescence. When the genotype II strains were present, Cas13a and Cas12b were activated simultaneously by *B646L* and *MGF* amplicons in a single reaction, producing yellow fluorescence (Figure 6B).

We first evaluated the analytical LOD of OBServe using serial dilutions of an equal molar mixture of plasmids containing either the genotype I or II *G1211R* sequence together with the *B646L* sequence. Notably, we found that OBServe could detect genotype I and II ASFVs, with an LOD of 1.6 copies/μL for both genotype ASFVs (Figure 6B), exhibiting a better performance in sensitivity compared with that in sensing wild-type and *MGF* gene-deleted ASFVs (1.6 copies/μL versus 8 copies/μL). We attributed this LOD variation to the sequence difference of RPA primers.

We further validated OBServe on 24 veterinary samples and detected ASFV from 14 of the 14 ASFV-positive samples tested, demonstrating 100% concordance with real-time PCR (Figures 5B and 5C, 6C). Among the 14 ASFV-positive samples, 13 of them were identified as genotype II, and 1 of them was identified as genotype I (Figure 6C). Interestingly, this genotype I ASFV is exactly the one that lacks *MGF* gene and we previously showed in Figure 5B. To further confirm this result, all ASFV-positive samples were typed using conventional PCR-sequencing method.[62] We demonstrated that the result of OBServe is consistent with the phylogenetic analysis (Figure 6D). Collectively, we developed a fast, sensitive, and field-deployable approach for the differentiation of genotype I and II ASFVs based on the OBServe platform.

DISCUSSION

Due to the lack of an approved vaccine or drug, ASF control primarily relies on the early diagnosis and culling of infected animals.[60] However, the efficacy of this strategy is weakened by the emergence of ASFV variants, including *MGF505-2R* gene-deleted ASFV[29] and low virulent genotype I ASFV,[28,30] as some of them cause mild onset of infection, chronic disease signs, and low-level viremia, which makes early diagnosis more challenging.[28] Moreover, infected pigs continuously shed viruses via oral and rectal routes, which leads to the spreading of asymptomatic infection and thus pose a great threat to the pig farm.[28,63] Therefore, optimizing sampling schemes and strengthening ASFV variants monitoring are urgently needed to minimize the losses caused by ASF.

Currently, several research groups have developed real-time PCR assays for identification of ASFV variants, targeting gene *B646L*,[59] *EP402R*,[64] *MGF505-2R*,[32] *MGF360-14L*,[58] *I117L*,[29] *E296R*,[24] and *E183L*.[33] Among these genes, *EP402R*[28,63] and *MGF 505-2R*[28–30] were frequently found missing in ASFV field isolates in China. Although *EP402R* is the most important virulence gene in ASFV, whose influence on virulence is irreplaceable,[65] it is not suitable for development of nucleic acid detection assays, as it shows high level of sequence variability, which may come from the selective pressure of the host immune system.[52] In contrast, *MGF505-2R* is relatively stable in the prevalent ASFV in China.[63]This can be explained by the fact that *MGF505-2R* did not show high antigenicity in sera from survived pigs infected with wild-type ASFV,[66] which means it somehow escaped the selective pressure from humoral immune response.

Therefore, by targeting the *MGF505-2R* gene and the highly conserved *B646L* gene, combining with CRISPR-Dx, the next-generation diagnostic tool,[67] we developed a dual-gene detection assay for discriminating between highly lethal wild-type and *MGF505-2R* gene-deleted ASFVs. In this technique, we developed a sensitive and fast dual-gene detection assay with minimal equipment requirement by taking advantage of Cas12b and Cas13a with regards to their orthogonal collateral cleavage preference against ssDNA and ssRNA probes, respectively, coupling it with multiplex RPA preamplification, and visualizing the readout via in-tube fluorescence or lateral flow strip (Figure 1).

To date, almost all CRISPR-Dxs that use lateral flow readout involve a short oligonucleotide reporter carrying a biotin molecule and a gold nanoparticle complex on separated ends.[8,44,68] On the lateral flow strips, a streptavidin-coated line will bind to biotin and capture all intact reporters to form a clear visible control band. However, a high target concentration in the sample leads to an invisible control band[69,70] because strong collateral cleavage activity upon target recognition degrades almost all probes, making differentiating between positive results and invalid lateral flow tests challenging.

In this study, we designed two oligonucleotide probes based on the working principle of HybriDetect 2T (Figure 2B). A disappearing test band was interpreted as a positive result, while a clear visible color on the test line was considered a negative result (Figure 2C). In particular, we lowered the total concentration of probes, resulting in excessive gold nanoparticles flowing over the control band, forming a clear visible color for validating the test run. The downside of our lateral flow assay is that using an absent test band to indicate positive results may cause a slightly higher false-negative rate, especially when detecting low viral load samples.

To our knowledge, the sensitivity of CRISPR-Dx is mainly dependent on the efficiency of preamplification because, for example, AapCas12b did not produce a detectable signal when the target double-strand DNA concentration was lower than 8 nM.[53] Therefore, we screened hundreds of sets of primers, successfully developing a robust multiplex RPA, yielding an assay that has the same sensitivity using either fluorescence or lateral flow strip readout (Figures 4, 5, and 6). However, the time-consuming and labor-intensive process of primer screening can be avoided by concentrating the sample[68,71] or using ultra-sensitive readout systems.[72] For instance, Joung et al. significantly enhanced the sensitivity of STOPCovid by increasing the sample input through magnetic beads-mediated sample concentration.[68] This strategy resulted in a 1,200-fold increase in sample input (2.5 μL input in routine nucleic acid amplification assay VS 3 mL input in STOPCovid).[68] Besides magnetic beads, other nanomaterials such as gold nanoparticles,[73] quantum dots,[74] and graphene oxide[75] are widely employed to construct ultra-sensitive biosensors for CRISPR-Dx or enable simple colorimetric visualization of test result. However, these commonly used nanomaterials are typically fabricated via physical or chemical methods, involving the use of toxic chemicals and high temperatures.[76] To address this concern, the principles of green chemistry have been integrated into the synthesis procedure of nanoparticles.[77] For example, magnetic nanoparticles have been successfully synthesized using plants,[78] bacteria,[79] algae,[80] and fungi.[81] We believe that the advancement of green nanotechnology will provide a more affordable, cleaner, safer, and eco-friendly approach to drive the future development of CRISPR-Dx.

In the multiplex RPA reaction, some primers dominate other primers due to the inherent base bias of the recombinases.[46] Hence, we systematically optimized the primer sequences, primer set combinations, concentration ratios, and total primer amounts in the reaction, ultimately yielding a balanced amplification efficiency (Figure 3).

Compared with the previously reported CRISPR-Cas-based dual-gene detection system, the biggest advantage of OBServe is replacing the commonly used LbCas12a with AapCas12b. AapCas12b is a newly identified thermostable Cas12 ortholog that has simpler PAM requirements and higher sensitivity and specificity.[53,68] In addition, the LbCas12a assay was inefficient when LbuCas13a and LbCas12a assays were combined in a single reaction.[50] In this study, we employed AapCas12b, together with an additional heating step to deactivate the Cas13a assay components[55] while enhancing the activity of Cas12b, generating a balanced signal in both the Cas13a detection channel and Cas12b detection channel (Figures 4, 5, and 6).

Having established the OBServe, we evaluated its performance on synthetic plasmid templates and veterinary samples via fluorescence and lateral flow readout, demonstrating 100% sensitivity and 100% specificity compared with triplex real-time PCR (Figures 5A–5D) with a sample-to-answer time less than 1 h. We also showed that OBServe did not cross-react with ten other common swine pathogens (Figure 5E). Featured with the multiplexed gene detection, visual readouts, limited equipment requirement, and accurate and quick turnaround time, OBServe could facilitate its use in a wider range of point-of-care settings for detection of ASFV and other pathogens.

Notably, we found an *MGF505-2R* gene-deleted ASFV in the field samples as shown in Figure 5B, but we could not confirm whether it was low virulent genotype I ASFV[28] or gene-deleted genotype II ASFV with unknown virulence. Therefore, we designed another dual-gene detection assay based on the working principle of OBServe to differentiate genotype I and II ASFVs by sensing a single-nucleotide polymorphism (SNP) in the PAM region of the Cas12b (Figure 6A). An attractive feature of CRISPR-Dx is the single-nucleotide specificity of the Cas enzyme, which enables viral variants that differ by only a single base or point mutations to be distinguished, which is challenging for conventional amplification-based detection approaches.

Consisting with the results of multiplex real-time PCR and phylogenetic analysis based on *B646L* gene sequence, OBServe classified 13 ASFV field isolates into genotype II, and grouped the *MGF505-2R* gene-deleted ASFV isolate into genotype I (Figures 6C and 6D). Noteworthy, in 2021, a genotype I ASFV with *MGF505-2R* gene deletion, HeN/ZZ-P1/21, was isolated from a pig farm in Henan Province in China.[28] Considering the similarity of gene loss pattern and sample source, our genotype I ASFV and HeN/ZZ-P1/21 may be derived from the same origin, but this assumption requires further validation using whole-genome sequencing approach.

In May 2023, Zhao et al. reported the isolation of three high lethal recombinant ASFVs with mosaic genomics composed of 56.5% highly virulent Georgia07-like genotype II virus and 43.5% low virulent NH/P68-like genotype I virus.[31] These new-emerging isolates may pose a serious challenge to the existing real-time PCR based ASFV genotyping methods. For example, these recombinant ASFVs will be classified into genotype I when using the standard *B646L* gene sequencing-based genotyping method,[62] for their *B646L* gene is derived from genotype I virus.[31] In contrast, recombinant ASFVs will mistakenly be classified into genotype II according to the recently developed real-time PCR based methods, which target the *E183L* gene[33] or *E296R* gene,[4,24] since the *E183L* and *E296R* genes of recombinant ASFVs are both derived from genotype II virus.[31]

Unfortunately, our OBServe will mistakenly group these recombinant ASFVs into genotype II too, as the *G1211R* gene of recombinant ASFVs that we targeted is derived from genotype II virus.[31] However, the initial goal of this study is to monitor the *MGF505-2R* gene-deleted ASFV and identify their genotype further. These recombinant ASFVs are out of the scope of this study. In addition, these recombinant ASFVs will be classified into highly virulent wild-type ASFV according to our method, which is consistent with its highly lethal phenotype.[31] Noteworthy, new reassortants with unknown virulence among low virulent genotype I ASFV and *MGF505-2R* gene-deleted genotype II ASFV, and recombinant ASFVs may subsequently emerge in the field.[28]

In summary, we have developed an extraction-free, rapid, and sensitive on-site dual-gene detection assay, OBServe, for the differentiation of *MGF505-2R* gene-deleted ASFV from wild-type ASFV, and provides a means to discriminate between genotype I and II ASFVs. OBServe has some advantages, including rapid testing (less than 1 h), sensitive testing (LOD down to 1.6 copies/μL), multiplexed detection capability, and minimal equipment requirements.

In addition to the veterinary applications explored in this study, OBServe can also be utilized for the detection of human pathogens and nucleic acid biomarkers associated with human diseases. For example, several dual-gene detection assays based on orthogonal CRISPR-Cas12a/Cas13a system have been developed to detect SARS-CoV-2 virus in clinical samples.[44,50,55,69] Furthermore, CRISPR-Dx has been employed for the detection of no-infectious diseases such as acute cellular kidney-transplant rejection,[82] medulloblastoma,[83] and breast cancer.[84] By eliminating the incompatibility between Cas12 and Cas13 systems, our orthogonal detection assay exhibits significantly enhanced signals (Figures 4A; S6), suggesting improved performance in future biomedical applications. Additionally, the single-nucleotide specificity of OBServe enables the detection of point mutations associated with drug resistance,[41] mutations related to Duchenne muscular dystrophy,[85] and disease-related miRNAs that can differ by only a single base.[41]

Electrochemical biosensors offer a green, rapid, highly sensitive, and cost-effective approach for detecting small molecules,[86–89] proteins,[90] nucleic acids,[83] and pathogens.[91] Leveraging the ultra-sensitive nature of electrochemical biosensors, OBServe holds the potential to eliminate the requirement for expensive and time-consuming preamplification process. The feasibility of this concept has been partially demonstrated through the development of amplification-free single-plex CRISPR-Dx utilizing electrochemical technology.[92,93]

Limitations of the study

There are some issues that need to be addressed in the future. (1) Integrating preamplification and CRISPR-Cas-based detection into a single reaction will eliminate the high-risk liquid transfer step between them. Although several single-plex, one-pot detection assays based

on Cas13a,[69] Cas12a,[40,94] and Cas12b[68] have been reported recently, their sensitivity is compromised, and requires an additional optimization process. (2) Both fluorescence and lateral flow readouts have tradeoffs between equipment requirements (for exciting the fluorophore) and cross-contamination risk derived from opening reaction tubes for each sample (lateral flow strips need to be manually inserted into reaction tubes). The obvious color change of the reaction solution will be an ideal form of signal output.[95] (3) Lyophilization of the reaction formulation will allow for a larger input volume, protect vulnerable RNA molecules, and facilitate their distribution for field applications. (4) To ensure consistent results between the on-site genotyping and the classic *B646L* genotyping based on Sanger sequencing, future work should design primers and probes/guide RNAs on the ASFV genotyping region, that is the C-terminus of the *B646L* gene with 478 bp.

STAR★METHODS

Detailed methods are provided in the online version of this paper and include the following:

- KEY RESOURCES TABLE
- RESOURCE AVAILABILITY
  - Lead contact
  - Materials availability
  - Data and code availability
- EXPERIMENTAL MODEL AND STUDY PARTICIPANT DETAILS
  - Common swine pathogens and veterinary sample collection
- METHOD DETAILS
  - Primers, plasmids and probes
  - Sample processing
  - Conservation analysis of OBServe targeting sites
  - Multiplex RPA of ASFV genes *B646L* and *MGF505-2R*
  - Cas enzyme expression and purification
  - crRNA preparation
  - Characterization of target dsDNA cleavage and collateral cleavage activity of AapCas12b and LwaCas13a
  - Orthogonal CRISPR-Cas12/Cas13 detection assay
  - Detection via lateral flow strips
  - Real-time PCR of ASFV
  - Conventional PCR, Sanger sequencing and multiple sequence alignment
- QUANTIFICATION AND STATISTICAL ANALYSIS

SUPPLEMENTAL INFORMATION

Supplemental information can be found online at https://doi.org/10.1016/j.isci.2024.109050.

ACKNOWLEDGMENTS

This work was supported by the Hainan Yazhou Bay Seed Laboratory (B21HJ0103), the Shandong Provincial Key R&D Program of China (2021LZGC001), the National Science Fund for Distinguished Young Scholars (31925036) and the National Key Research and Development Program of China (2021YFD1801301, 2020YFA0509503, 2022YFF0710703, 2021YFA0805902).

AUTHOR CONTRIBUTIONS

Conceptualization: Y.F.W., G.P.Z., J.G.Z., and Z.W.; methodology: Y.W., Y.Z., and Z.W.; investigation: Z.W.; resources: G.S.Q., W.B.S., and A.P.W.; writing – original draft: Z.W.; writing – review and editing: Z.W. and J.G.Z.; visualization: Z.W.; supervision: A.P.W., Y.F.W., G.P.Z., and J.G.Z.; funding acquisition: A.P.W., Y.F.W., G.P.Z., and J.G.Z.

DECLARATION OF INTERESTS

The authors declare no competing interests.

Received: October 9, 2023
Revised: December 14, 2023
Accepted: January 23, 2024
Published: March 7, 2024

REFERENCES

1. Aicher, S.-M., Monaghan, P., Netherton, C.L., and Hawes, P.C. (2021). Unpicking the secrets of African swine fever viral replication sites. Viruses *13*, 77.
2. Gallardo, C., Fernández-Pinero, J., and Arias, M. (2019). African swine fever (ASF) diagnosis, an essential tool in the epidemiological investigation. Virus Res. *271*, 197676.
3. Chen, W., Zhao, D., He, X., Liu, R., Wang, Z., Zhang, X., Li, F., Shan, D., Chen, H., Zhang, J., et al. (2020). A seven-gene-deleted African swine fever virus is safe and effective as a live attenuated vaccine in pigs. Sci. China Life Sci. *63*, 623–634.
4. Song, R., Liu, P., Yang, Y., Lee, H.S., Chen, C., Wu, X., and Li, X. (2022). Development of a Duplex Insulated Isothermal PCR Assay for Rapid On-Site Detection and Differentiation of Genotypes 1 and 2 of African Swine Fever Virus. Front. Cell. Infect. Microbiol. *12*, 961.
5. Wang, N., Zhao, D., Wang, J., Zhang, Y., Wang, M., Gao, Y., Li, F., Wang, J., Bu, Z., Rao, Z., and Wang, X. (2019). Architecture of African swine fever virus and implications for viral assembly. Science *366*, 640–644.
6. Dixon, L.K., Sun, H., and Roberts, H. (2019). African swine fever. Antivir. Res. *165*, 34–41.
7. Njau, E.P., Domelevo Entfellner, J.-B., Machuka, E.M., Bochere, E.N., Cleaveland, S., Shirima, G.M., Kusiluka, L.J., Upton, C., Bishop, R.P., Pelle, R., and Okoth, E.A. (2021). The first genotype II African swine fever virus isolated in Africa provides insight into the current Eurasian pandemic. Sci. Rep. *11*, 13081.
8. Lu, S., Li, F., Chen, Q., Wu, J., Duan, J., Lei, X., Zhang, Y., Zhao, D., Bu, Z., and Yin, H. (2020). Rapid detection of African swine fever virus using Cas12a-based portable paper diagnostics. Cell Discov. *6*, 18.
9. Boinas, F.S., Hutchings, G.H., Dixon, L.K., and Wilkinson, P.J. (2004). Characterization of pathogenic and non-pathogenic African swine fever virus isolates from Ornithodoros erraticus inhabiting pig premises in Portugal. J. Gen. Virol. *85*, 2177–2187.
10. Leitão, A., Cartaxeiro, C., Coelho, R., Cruz, B., Parkhouse, R.M.E., Portugal, F.C., Vigário, J.D., and Martins, C.L.V. (2001). The non-haemadsorbing African swine fever virus isolate ASFV/NH/P68 provides a model for defining the protective anti-virus immune response. J. Gen. Virol. *82*, 513–523.
11. King, K., Chapman, D., Argilaguet, J.M., Fishbourne, E., Hutet, E., Cariolet, R., Hutchings, G., Oura, C.A.L., Netherton, C.L., Moffat, K., et al. (2011). Protection of European domestic pigs from virulent African isolates of African swine fever virus by experimental immunisation. Vaccine *29*, 4593–4600.
12. Mulumba-Mfumu, L., Goatley, L.C., Saegerman, C., Takamatsu, H.H., and Dixon, L.K. (2016). Immunization of African indigenous pigs with attenuated genotype I African swine fever virus OURT 88/3 induces protection against challenge with virulent strains of genotype I. Transbound. Emerg. Dis. *63*, e323–e327.
13. O'Donnell, V., Holinka, L.G., Gladue, D.P., Sanford, B., Krug, P.W., Lu, X., Arzt, J., Reese, B., Carrillo, C., Risatti, G.R., and Borca, M.V. (2015). African swine fever virus Georgia isolate harboring deletions of MGF360 and MGF505 genes is attenuated in swine and confers protection against challenge with virulent parental virus. J. Virol. *89*, 6048–6056.
14. Reis, A.L., Abrams, C.C., Goatley, L.C., Netherton, C., Chapman, D.G., Sanchez-Cordon, P., and Dixon, L.K. (2016). Deletion of African swine fever virus interferon inhibitors from the genome of a virulent isolate reduces virulence in domestic pigs and induces a protective response. Vaccine *34*, 4698–4705.
15. Sánchez-Cordón, P.J., Jabbar, T., Berrezaie, M., Chapman, D., Reis, A., Sastre, P., Rueda, P., Goatley, L., and Dixon, L.K. (2018). Evaluation of protection induced by immunisation of domestic pigs with deletion mutant African swine fever virus BeninΔMGF by different doses and routes. Vaccine *36*, 707–715.
16. Monteagudo, P.L., Lacasta, A., López, E., Bosch, L., Collado, J., Pina-Pedrero, S., Correa-Fiz, F., Accensi, F., Navas, M.J., Vidal, E., et al. (2017). BA71ΔCD2: a new recombinant live attenuated African swine fever virus with cross-protective capabilities. J. Virol. *91*. e01058-17.
17. Yang, H., Peng, Z., Song, W., Zhang, C., Fan, J., Chen, H., Hua, L., Pei, J., Tang, X., Chen, H., and Wu, B. (2022). A triplex real-time PCR method to detect African swine fever virus gene-deleted and wild type strains. Front. Vet. Sci. *9*, 943099.
18. Liu, Y., Xie, Z., Li, Y., Song, Y., Di, D., Liu, J., Gong, L., Chen, Z., Wu, J., Ye, Z., et al. (2023). Evaluation of an I177L gene-based five-gene-deleted African swine fever virus as a live attenuated vaccine in pigs. Emerg. Microb. Infect. *12*, 2148560.
19. Borca, M.V., Holinka, L.G., Berggren, K.A., and Gladue, D.P. (2018). CRISPR-Cas9, a tool to efficiently increase the development of recombinant African swine fever viruses. Sci. Rep. *8*, 3154.
20. Mushagalusa, C.A., Etter, E., and Penrith, M.-L. (2021). Review of African swine fever outbreaks history in South Africa: From 1926 to 2018. Onderstepoort J. Vet. Res. *88*, 1–10.
21. Cisek, A.A., Dąbrowska, I., Gregorczyk, K.P., and Wyżewski, Z. (2016). African swine fever virus: a new old enemy of Europe. Ann. Parasitol. *62*, 161–167.
22. Revilla, Y., Pérez-Núñez, D., and Richt, J.A. (2018). African swine fever virus biology and vaccine approaches. Adv. Virus Res. *100*, 41–74.
23. Gao, L., Sun, X., Yang, H., Xu, Q., Li, J., Kang, J., Liu, P., Zhang, Y., Wang, Y., and Huang, B. (2021). Epidemic situation and control measures of African Swine Fever Outbreaks in China 2018–2020. Transbound. Emerg. Dis. *68*, 2676–2686.
24. Li, X., Hu, Y., Liu, P., Zhu, Z., Liu, P., Chen, C., and Wu, X. (2022). Development and application of a duplex real-time PCR assay for differentiation of genotypes I and II African swine fever viruses. Transbound. Emerg. Dis. *69*, 2971–2979.
25. Tao, D., Sun, D., Liu, Y., Wei, S., Yang, Z., An, T., Shan, F., Chen, Z., and Liu, J. (2020). One year of African swine fever outbreak in China. Acta Trop. *211*, 105602.
26. Li, X., and Tian, K. (2018). African swine fever in China. Vet. Rec. *183*, 300–301.
27. Zhao, D., Liu, R., Zhang, X., Li, F., Wang, J., Zhang, J., Liu, X., Wang, L., Zhang, J., Wu, X., et al. (2019). Replication and virulence in pigs of the first African swine fever virus isolated in China. Emerg. Microb. Infect. *8*, 438–447.
28. Sun, E., Huang, L., Zhang, X., Zhang, J., Shen, D., Zhang, Z., Wang, Z., Huo, H., Wang, W., Huangfu, H., et al. (2021). Genotype I African swine fever viruses emerged in domestic pigs in China and caused chronic infection. Emerg. Microb. Infect. *10*, 2183–2193.
29. Zhao, K., Shi, K., Zhou, Q., Xiong, C., Mo, S., Zhou, H., Long, F., Wei, H., Hu, L., and Mo, M. (2022). The Development of a Multiplex Real-Time Quantitative PCR Assay for the Differential Detection of the Wild-Type Strain and the MGF505-2R, EP402R and I177L Gene-Deleted Strain of the African Swine Fever Virus. Animals *12*, 1754.
30. Shi, K., Liu, H., Yin, Y., Si, H., Long, F., and Feng, S. (2022). Molecular characterization of African swine fever virus from 2019-2020 outbreaks in Guangxi Province, Southern China. Front. Vet. Sci. *9*, 912224.
31. Zhao, D., Sun, E., Huang, L., Ding, L., Zhu, Y., Zhang, J., Shen, D., Zhang, X., Zhang, Z., Ren, T., et al. (2023). Highly lethal genotype I and II recombinant African swine fever viruses detected in pigs. Nat. Commun. *14*, 3096.
32. Guo, Z., Li, K., Qiao, S., Chen, X.X., Deng, R., and Zhang, G. (2020). Development and evaluation of duplex TaqMan real-time PCR assay for detection and differentiation of wide-type and MGF505-2R gene-deleted African swine fever viruses. BMC Vet. Res. *16*, 428–429.
33. Gao, Q., Feng, Y., Yang, Y., Luo, Y., Gong, T., Wang, H., Gong, L., Zhang, G., Zheng, Z., and Gong, L. (2022). Establishment of a dual real-time PCR assay for the identification of African swine fever virus genotypes I and II in China. Front. Vet. Sci. *9*.
34. Cao, S., Lu, H., Wu, Z., and Zhu, S. (2022). A duplex fluorescent quantitative PCR assay to distinguish the genotype I and II strains of African swine fever virus in Chinese epidemic strains. Front. Vet. Sci. *9*, 998874.
35. Ilya, T., Monoldorova, S., Kang, S.-S., Yun, S., Byeon, H.-S., Mariia, N., and Jeon, B.-Y. (2022). Development of a Real-Time Recombinase Polymerase Amplification Assay for the Rapid Detection of African Swine Fever Virus Genotype I and II. Pathogens *11*, 439.
36. Sastre, P., Gallardo, C., Monedero, A., Ruiz, T., Arias, M., Sanz, A., and Rueda, P. (2016). Development of a novel lateral flow assay for detection of African swine fever in blood. BMC Vet. Res. *12*, 206–208.
37. Wang, Z.-H., Li, P., Lin, X., Jia, H., Jiang, Y.-T., Wang, X.-J., and Hou, S.-H. (2021). Application of portable real-time recombinase-aided amplification (rt-RAA) assay in the clinical diagnosis of ASFV and prospective DIVA diagnosis. Appl. Microbiol. Biotechnol. *105*, 3249–3264.
38. Zhang, Y., Li, Q., Guo, J., Li, D., Wang, L., Wang, X., Xing, G., Deng, R., and Zhang, G. (2021). An isothermal molecular point of care testing for African swine fever virus using recombinase-aided amplification and lateral flow assay without the need to extract nucleic acids in blood. Front. Cell. Infect. Microbiol. *11*, 633763.
39. Wang, Y., Dai, J., Liu, Y., Yang, J., Hou, Q., Ou, Y., Ding, Y., Ma, B., Chen, H., Li, M., et al. (2021). Development of a potential penside colorimetric LAMP assay using neutral red for detection of African swine fever virus. Front. Microbiol. *12*, 609821.
40. Hu, M., Qiu, Z., Bi, Z., Tian, T., Jiang, Y., and Zhou, X. (2022). Photocontrolled crRNA activation enables robust CRISPR-Cas12a diagnostics. Proc. Natl. Acad. Sci. USA *119*, e2202034119.

41. Kaminski, M.M., Abudayyeh, O.O., Gootenberg, J.S., Zhang, F., and Collins, J.J. (2021). CRISPR-based diagnostics. Nat. Biomed. Eng. *5*, 643–656.
42. Chen, J.S., Ma, E., Harrington, L.B., Da Costa, M., Tian, X., Palefsky, J.M., and Doudna, J.A. (2018). CRISPR-Cas12a target binding unleashes indiscriminate single-stranded DNase activity. Science *360*, 436–439.
43. Gootenberg, J.S., Abudayyeh, O.O., Lee, J.W., Essletzbichler, P., Dy, A.J., Joung, J., Verdine, V., Donghia, N., Daringer, N.M., Freije, C.A., et al. (2017). Nucleic acid detection with CRISPR-Cas13a/C2c2. Science *356*, 438–442.
44. Su, G., Zhu, M., Li, D., Xu, M., Zhu, Y., Zhang, Y., Zhu, H., Li, F., and Yu, Y. (2022). Multiplexed lateral flow assay integrated with orthogonal CRISPR-Cas system for SARS-CoV-2 detection. Sensor. Actuator. B Chem. *371*, 132537.
45. Nalefski, E.A., Patel, N., Leung, P.J.Y., Islam, Z., Kooistra, R.M., Parikh, I., Marion, E., Knott, G.J., Doudna, J.A., Le Ny, A.-L.M., and Madan, D. (2021). Kinetic analysis of Cas12a and Cas13a RNA-Guided nucleases for development of improved CRISPR-Based diagnostics. iScience *24*, 102996.
46. Kellner, M.J., Koob, J.G., Gootenberg, J.S., Abudayyeh, O.O., and Zhang, F. (2019). SHERLOCK: nucleic acid detection with CRISPR nucleases. Nat. Protoc. *14*, 2986–3012.
47. Ai, J.W., Zhou, X., Xu, T., Yang, M., Chen, Y., He, G.Q., Pan, N., Cai, Y., Li, Y., Wang, X., et al. (2019). CRISPR-based rapid and ultra-sensitive diagnostic test for Mycobacterium tuberculosis. Emerg. Microb. Infect. *8*, 1361–1369.
48. Mukama, O., Yuan, T., He, Z., Li, Z., Habimana, J.d.D., Hussain, M., Li, W., Yi, Z., Liang, Q., and Zeng, L. (2020). A high fidelity CRISPR/Cas12a based lateral flow biosensor for the detection of HPV16 and HPV18. Sensor. Actuator. B Chem. *316*, 128119.
49. Yang, B., Shi, Z., Ma, Y., Wang, L., Cao, L., Luo, J., Wan, Y., Song, R., Yan, Y., Yuan, K., et al. (2022). LAMP assay coupled with CRISPR/Cas12a system for portable detection of African swine fever virus. Transbound. Emerg. Dis. *69*, e216–e223.
50. Tian, T., Qiu, Z., Jiang, Y., Zhu, D., and Zhou, X. (2022). Exploiting the orthogonal CRISPR-Cas12a/Cas13a trans-cleavage for dual-gene virus detection using a handheld device. Biosens. Bioelectron. *196*, 113701.
51. Gootenberg, J.S., Abudayyeh, O.O., Kellner, M.J., Joung, J., Collins, J.J., and Zhang, F. (2018). Multiplexed and portable nucleic acid detection platform with Cas13, Cas12a, and Csm6. Science *360*, 439–444.
52. Bao, Y.J., Qiu, J., Luo, Y., Rodríguez, F., and Qiu, H.J. (2021). The genetic variation landscape of African swine fever virus reveals frequent positive selection and adaptive flexibility. Transbound. Emerg. Dis. *68*, 2703–2721.
53. Teng, F., Guo, L., Cui, T., Wang, X.-G., Xu, K., Gao, Q., Zhou, Q., and Li, W. (2019). CDetection: CRISPR-Cas12b-based DNA detection with sub-attomolar sensitivity and single-base specificity. Genome Biol. *20*, 132–137.
54. Teng, F., Cui, T., Feng, G., Guo, L., Xu, K., Gao, Q., Li, T., Li, J., Zhou, Q., and Li, W. (2018). Repurposing CRISPR-Cas12b for mammalian genome engineering. Cell Discov. *4*, 63.
55. Mahas, A., Marsic, T., Lopez-Portillo Masson, M., Wang, Q., Aman, R., Zheng, C., Ali, Z., Alsanea, M., Al-Qahtani, A., Ghanem, B., et al. (2022). Characterization of a thermostable Cas13 enzyme for one-pot detection of SARS-CoV-2. Proc. Natl. Acad. Sci. USA *119*, e2118260119.
56. Wang, X., Chen, Y., Cheng, X., Wang, S.-Q., Hu, Y., Feng, Y., Jin, R., Zhou, K., Liu, T., Wang, J., et al. (2023). CDetection. v2: One-pot assay for the detection of SARS-CoV-2. Front. Microbiol. *14*, 1158163.
57. Wang, Y., Xu, L., Noll, L., Stoy, C., Porter, E., Fu, J., Feng, Y., Peddireddi, L., Liu, X., Dodd, K.A., et al. (2020). Development of a real-time PCR assay for detection of African swine fever virus with an endogenous internal control. Transbound. Emerg. Dis. *67*, 2446–2454.
58. Lin, Y., Cao, C., Shi, W., Huang, C., Zeng, S., Sun, J., Wu, J., and Hua, Q. (2020). Development of a triplex real-time PCR assay for detection and differentiation of gene-deleted and wild-type African swine fever virus. J. Virol. Methods *280*, 113875.
59. Ding, L.l., Ren, T., Huang, L.y., Tesfagaber, W., Zhu, Y.m., Li, F., Sun, E.c., Bu, Z.g., and Zhao, D.m. (2023). Developing a duplex ARMS-qPCR method to differentiate genotype I and II African swine fever viruses based on their B646L genes. J. Integr. Agric. *22*, 1603–1607.
60. Galindo, I., and Alonso, C. (2017). African swine fever virus: a review. Viruses *9*, 103.
61. Dixon, L.K., Chapman, D.A.G., Netherton, C.L., and Upton, C. (2013). African swine fever virus replication and genomics. Virus Res. *173*, 3–14.
62. Bastos, A.D.S., Penrith, M.-L., Crucière, C., Edrich, J.L., Hutchings, G., Roger, F., Couacy-Hymann, E., and R Thomson, G. (2003). Genotyping field strains of African swine fever virus by partial p72 gene characterisation. Arch. Virol. *148*, 693–706.
63. Sun, E., Zhang, Z., Wang, Z., He, X., Zhang, X., Wang, L., Wang, W., Huang, L., Xi, F., Huangfu, H., et al. (2021). Emergence and prevalence of naturally occurring lower virulent African swine fever viruses in domestic pigs in China in 2020. Sci. China Life Sci. *64*, 752–765.
64. Zhu, J., Jian, W., Huang, Y., Gao, Q., Gao, F., Chen, H., Zhang, G., Liao, M., and Qi, W. (2022). Development and Application of a Duplex Droplet Digital Polymerase Chain Reaction Assay for Detection and Differentiation of EP402R-Deleted and Wild-Type African Swine Fever Virus. Front. Vet. Sci. *9*, 905706.
65. Wang, Z., Qi, C., Ge, S., Hu, Y., Zhang, X., Lv, Y., Han, N., Wu, X., Qian, Y., and Wang, Z. (2022). Genetic variation and evolution of attenuated African swine fever virus strain isolated in the field: A review. Virus Res. *319*, 198874.
66. Wang, L., Fu, D., Tesfagaber, W., Li, F., Chen, W., Zhu, Y., Sun, E., Wang, W., He, X., Guo, Y., et al. (2022). Development of an ELISA Method to Differentiate Animals Infected with Wild-Type African Swine Fever Viruses and Attenuated HLJ/18-7GD Vaccine Candidate. Viruses *14*, 1731.
67. Chertow, D.S. (2018). Next-generation diagnostics with CRISPR. Sci. Technol. Humanit. *360*, 381–382.
68. Joung, J., Ladha, A., Saito, M., Kim, N.-G., Woolley, A.E., Segel, M., Barretto, R.P.J., Ranu, A., Macrae, R.K., Faure, G., et al. (2020). Detection of SARS-CoV-2 with SHERLOCK one-pot testing. N. Engl. J. Med. *383*, 1492–1494.
69. Arizti-Sanz, J., Bradley, A., Zhang, Y.B., Boehm, C.K., Freije, C.A., Grunberg, M.E., Kosoko-Thoroddsen, T.-S.F., Welch, N.L., Pillai, P.P., Mantena, S., et al. (2022). Simplified Cas13-based assays for the fast identification of SARS-CoV-2 and its variants. Nat. Biomed. Eng. *6*, 932–943.
70. Broughton, J.P., Deng, X., Yu, G., Fasching, C.L., Servellita, V., Singh, J., Miao, X., Streithorst, J.A., Granados, A., Sotomayor-Gonzalez, A., et al. (2020). CRISPR–Cas12-based detection of SARS-CoV-2. Nat. Biotechnol. *38*, 870–874.
71. Nemudraia, A., Nemudryi, A., Buyukyoruk, M., Scherffius, A.M., Zahl, T., Wiegand, T., Pandey, S., Nichols, J.E., Hall, L.N., McVey, A., et al. (2022). Sequence-specific capture and concentration of viral RNA by type III CRISPR system enhances diagnostic. Nat. Commun. *13*, 7762.
72. Huang, Z., Lyon, C.J., Wang, J., Lu, S., and Hu, T.Y. (2023). CRISPR Assays for Disease Diagnosis: Progress to and Barriers Remaining for Clinical Applications. Adv. Sci. *10*, 2301697.
73. Jiang, Y., Hu, M., Liu, A.-A., Lin, Y., Liu, L., Yu, B., Zhou, X., and Pang, D.-W. (2021). Detection of SARS-CoV-2 by CRISPR/Cas12a-enhanced colorimetry. ACS Sens. *6*, 1086–1093.
74. Bao, M., Jensen, E., Chang, Y., Korensky, G., and Du, K. (2020). Magnetic bead-quantum dot (MB-qdot) clustered regularly interspaced short palindromic repeat assay for simple viral DNA detection. ACS Appl. Mater. Interfaces *12*, 43435–43443.
75. Cheng, X., Yan, Y., Chen, X., Duan, J., Zhang, D., Yang, T., Gou, X., Zhao, M., Ding, S., and Cheng, W. (2021). CRISPR/Cas12a-Modulated fluorescence resonance energy transfer with nanomaterials for nucleic acid sensing. Sensor. Actuator. B Chem. *331*, 129458.
76. Rani, M., and Shanker, U. (2022). Green nanomaterials: An overview. In Green Functionalized Nanomaterials for Environmental Applications, U. Shanker, C.M. Hussain, and M. Rani, eds. (Elsevier), pp. 43–80.
77. Priya, N., Kaur, K., and Sidhu, A.K. (2021). Green synthesis: An eco-friendly route for the synthesis of iron oxide nanoparticles. Front. Nanotech. *3*, 655062.
78. Vasantharaj, S., Sathiyavimal, S., Senthilkumar, P., LewisOscar, F., and Pugazhendhi, A. (2019). Biosynthesis of iron oxide nanoparticles using leaf extract of Ruellia tuberosa: antimicrobial properties and their applications in photocatalytic degradation. J. Photochem. Photobiol., B *192*, 74–82.
79. Jubran, A.S., Al-Zamely, O.M., and Al-Ammar, M.H. (2020). A study of iron oxide nanoparticles synthesis by using bacteria. ijpqa. *11*, 88–92.
80. Salem, D.M., Ismail, M.M., and Aly-Eldeen, M.A. (2019). Biogenic synthesis and antimicrobial potency of iron oxide (Fe3O4) nanoparticles using algae harvested from the Mediterranean Sea, Egypt. The Egyptian Journal of Aquatic Research *45*, 197–204.
81. Chatterjee, S., Mahanty, S., Das, P., Chaudhuri, P., and Das, S. (2020). Biofabrication of iron oxide nanoparticles using manglicolous fungus Aspergillus niger BSC-1 and removal of Cr (VI) from aqueous solution. Chem. Eng. J. *385*, 123790.

82. Kaminski, M.M., Alcantar, M.A., Lape, I.T., Greensmith, R., Huske, A.C., Valeri, J.A., Marty, F.M., Klämbt, V., Azzi, J., Akalin, E., et al. (2020). A CRISPR-based assay for the detection of opportunistic infections post-transplantation and for the monitoring of transplant rejection. Nat. Biomed. Eng. *4*, 601–609.
83. Bruch, R., Baaske, J., Chatelle, C., Meirich, M., Madlener, S., Weber, W., Dincer, C., and Urban, G.A. (2019). CRISPR/Cas13a-powered electrochemical microfluidic biosensor for nucleic acid amplification-free miRNA diagnostics. Adv. Mater. *31*, 1905311.
84. Sha, Y., Huang, R., Huang, M., Yue, H., Shan, Y., Hu, J., and Xing, D. (2021). Cascade CRISPR/cas enables amplification-free microRNA sensing with fM-sensitivity and single-base-specificity. Chem. Commun. *57*, 247–250.
85. Hajian, R., Balderston, S., Tran, T., DeBoer, T., Etienne, J., Sandhu, M., Wauford, N.A., Chung, J.-Y., Nokes, J., Athaiya, M., et al. (2019). Detection of unamplified target genes via CRISPR–Cas9 immobilized on a graphene field-effect transistor. Nat. Biomed. Eng. *3*, 427–437.
86. Eftekhari, A., Dalili, M., Karimi, Z., Rouhani, S., Hasanzadeh, A., Rostamnia, S., Khaksar, S., Idris, A.O., Karimi-Maleh, H., Yola, M.L., and Msagati, T.A.M. (2021). Sensitive and selective electrochemical detection of bisphenol A based on SBA-15 like Cu-PMO modified glassy carbon electrode. Food Chem. *358*, 129763.
87. Kavetskyy, T.S., Kukhazh, Y.Y., Zubrytska, K.V., Khalilov, R.I., Smutok, O.V., Demkiv, O.M., Šauša, O., Švajdlenková, H., and Gonchar, M.V. (2019). Construction of amperometric laccase-based biosensors using the ureasil and photocross-linked polymers. Advances in Biology & Earth Sciences *4*.
88. Wang, A., You, X., Liu, H., Zhou, J., Chen, Y., Zhang, C., Ma, K., Liu, Y., Ding, P., Qi, Y., and Zhang, G. (2022). Development of a label free electrochemical sensor based on a sensitive monoclonal antibody for the detection of tiamulin. Food Chem. *366*, 130573.
89. You, X., Zhang, G., Chen, Y., Liu, D., Ma, D., Zhou, J., Liu, Y., Liu, H., Qi, Y., Liang, C., et al. (2021). A novel electrochemical immunosensor for the sensitive detection of tiamulin based on staphylococcal protein A and silver nanoparticle-graphene oxide nanocomposites. Bioelectrochemistry *141*, 107877.
90. Dai, Y., Somoza, R.A., Wang, L., Welter, J.F., Li, Y., Caplan, A.I., and Liu, C.C. (2019). Exploring the trans-cleavage activity of CRISPR-Cas12a (cpf1) for the development of a universal electrochemical biosensor. Angew. Chem. *131*, 17560–17566.
91. Cesewski, E., and Johnson, B.N. (2020). Electrochemical biosensors for pathogen detection. Biosens. Bioelectron. *159*, 112214.
92. Balderston, S., Taulbee, J.J., Celaya, E., Fung, K., Jiao, A., Smith, K., Hajian, R., Gasiunas, G., Kutanovas, S., Kim, D., et al. (2021). Discrimination of single-point mutations in unamplified genomic DNA via Cas9 immobilized on a graphene field-effect transistor. Nat. Biomed. Eng. *5*, 713–725.
93. Shinoda, H., Taguchi, Y., Nakagawa, R., Makino, A., Okazaki, S., Nakano, M., Muramoto, Y., Takahashi, C., Takahashi, I., Ando, J., et al. (2021). Amplification-free RNA detection with CRISPR–Cas13. Commun. Biol. *4*, 476.
94. Lu, S., Tong, X., Han, Y., Zhang, K., Zhang, Y., Chen, Q., Duan, J., Lei, X., Huang, M., Qiu, Y., et al. (2022). Fast and sensitive detection of SARS-CoV-2 RNA using suboptimal protospacer adjacent motifs for Cas12a. Nat. Biomed. Eng. *6*, 286–297.
95. Arizti-Sanz, J., Freije, C.A., Stanton, A.C., Petros, B.A., Boehm, C.K., Siddiqui, S., Shaw, B.M., Adams, G., Kosoko-Thoroddsen, T.-S.F., Kemball, M.E., et al. (2020). Streamlined inactivation, amplification, and Cas13-based detection of SARS-CoV-2. Nat. Commun. *11*, 5921.
96. Qian, J., Boswell, S.A., Chidley, C., Lu, Z.-x., Pettit, M.E., Gaudio, B.L., Fajnzylber, J.M., Ingram, R.T., Ward, R.H., Li, J.Z., and Springer, M. (2020). An enhanced isothermal amplification assay for viral detection. Nat. Commun. *11*, 5920.
97. East-Seletsky, A., O'Connell, M.R., Knight, S.C., Burstein, D., Cate, J.H.D., Tjian, R., and Doudna, J.A. (2016). Two distinct RNase activities of CRISPR-C2c2 enable guide-RNA processing and RNA detection. Nature *538*, 270–273.

STAR★METHODS

KEY RESOURCES TABLE

REAGENT or RESOURCE	SOURCE	IDENTIFIER
Bacterial and Virus Strains		
E. coli BL21(DE3) Competent Cells	Biomed	Cat#BC201-2
PRRSV	Yuanquan Animal Health	Strain CH-1R
JEV	Yuanquan Animal Health	Strain SA14-14-2
CSFV	Yuanquan Animal Health	Tissue culture origin
PEDV	Yuanquan Animal Health	Strain LW
PPV	Yuanquan Animal Health	Strain S-1
PCV2	Yuanquan Animal Health	Strain LG
PRV	Yuanquan Animal Health	Strain Bartha-61
Swine Erysipelas	Yuanquan Animal Health	Strain G4T10
Swine Salmonellosis	Yuanquan Animal Health	Strain E0630
TGEV	Yuanquan Animal Health,	Strain SD/L
E. coli Rosetta 2 (DE3) pLysS	Merck	Cat#71401-3
Biological Samples		
ASFV field samples	Henan Center for Animal Disease Control and Prevention, China	N/A
Chemicals, Peptides, and Recombinant Proteins		
AapCas12b	This study	N/A
LwaCas13a	This study	N/A
cOmplete, EDTA-free	Roche	Cat#4693132001
IPTG	BBI	Cat#A600168
UltraNuclease	Yeasen Biotech	Cat#20156ES25
Step-Tactin XT 4Flow high-capacity resin	IBA Life Science	Cat#2-5030-002
SUMO Protease	Biomed	Cat# PA130-02
IGEPAL CA-630	Sigma-Aldrich	Cat# I8896-50ML
SP Sepharose fast flow	Cytiva	Cat#17172910
Ni NTA Beads 6FF	Lablead	Cat#N30210
D-Biotin	BBI	Cat#A600078
Murine RNase Inhibitor	Vazyme	Cat# R301-03
NEBuffer 1.1	NEB	Cat#B7201S
NEBuffer 2.1	NEB	Cat#B7202S
NEBuffer 3.1	NEB	Cat# B7203S
CutSmart	NEB	Cat# B7204S
SHINE buffer	Arizti-Sanz et al., 2020[95]	N/A
NxGenT7 RNA polymerase	Lucigen	Cat#30223-1
rNTPs mix	Thermo Fisher Scientific	Cat#R0481
DNase/RNase-Free water	TIANGEN	Cat#RT121-01
2×Phanta Max Master Mix	Vazyme	Cat#P525-02
Critical Commercial Assays		
Fast DNA extraction solution	Zhongdao Biotech	Cat#P1723
TIANamp virus DNA/RNA kit	TIANGEN	Cat#DP315-F

(*Continued on next page*)

Continued

REAGENT or RESOURCE	SOURCE	IDENTIFIER
RPA Nucleic Acid Amplification Kit	Qitian	Cat#B00000
T7 High RNA Transcription kit	Vazyme	Cat# TR101-01
VAHTS RNA Clean Beads	Vazyme	Cat#N412-01-AA
HybriDetect 2T	Milenia	Cat#MGDS2A
Single-plex real-time PCR kit	Zhongdao Biotech	Cat#P1723
Triplex real-time PCR kit	Lijian	ASFV-q50T 3.0
Oligonucleotides		
Sequence of RPA primers, see Table S1	This study	N/A
Sequence of crRNAs, see Table S2	This study	N/A
Sequence of probes, see Table S3	This study	N/A
Recombinant DNA		
pC013-Twinstrep-SUMO-huLwaCas13a	Addgene#90097	Gootenberg et al., 2017[43]
p72-pPUR-TPA-ASFV-Fc	This study	N/A
BPK2014-Cas12b	Wei Li	Teng et al., 2019[53]
pY016 (pcDNA3.1-hLbCpf1)	Haoyi Wang	N/A
pC013-Twinstrep-SUMO-LbCas12a	This study	N/A
pUC57-MGF505-2R	This study	N/A
pUC57-G1211R-genotype I	This study	N/A
pUC57-G1211R-genotype II	This study	N/A
Software and Algorithms		
MEGA (version: 10.2.5)	https://www.megasoftware.net	N/A
Adobe Photoshop CS	https://www.adobe.com	N/A
GraphPad Prism 7	https://www.graphpad.com	N/A
Biorender	https://www.biorender.com	N/A

RESOURCE AVAILABILITY

Lead contact

Further information and requests for resources and reagents should be directed to and will be fulfilled by the lead contact, Jianguo Zhao (zhaojg@ioz.ac.cn).

Materials availability

This study did not generate unique reagents.

Data and code availability

- All data reported in this paper will be shared by the lead contact upon request.
- This paper does not report original code.
- Any additional information required to reanalyze the data reported in this paper is available from the lead contact upon request.

EXPERIMENTAL MODEL AND STUDY PARTICIPANT DETAILS

Common swine pathogens and veterinary sample collection

Porcine reproductive and respiratory syndrome virus (PRRSV, strain CH-1R), Japanese encephalitis virus (JEV, strain SA14-14-2), classical swine fever virus (CSFV, tissue culture origin), porcine epidemic diarrhea virus (PEDV, strain LW), porcine parvovirus (PPV, strain S-1), porcine circovirus type 2 (PCV2, strain LG), pseudorabies virus (PRV, strain Bartha-61), swine erysipelas (SE, strain G4T10), swine salmonellosis (SS, strain E0630), and transmissible gastroenteritis virus (TGEV, strain SD/L) are commonly used and commercially available vaccine strains of swine in China that were purchased from Yuanquan Animal Health (Chongqing, China).

Swine blood samples and swab samples were collected by Henan Center for Animal Disease Control and Prevention, Zhengzhou, China. All veterinary samples were inactivated at 70°C for 30 minutes before transport and sample processing. After experiments, all related materials were destroyed by high-temperature and high-pressure treatments according to biosafety operation specifications.

METHOD DETAILS

Primers, plasmids and probes

All primers were ordered from Sangon Biotech (Shanghai, China) or Tsingke Biotech (Beijing, China). Detailed primer sequences are listed in Table S1. Forward RPA primers for the *B646L* gene were designed with a T7 promoter sequence appended upstream.

The ASFV genes *MGF505-2R*, *G1211R*-genotype I, and *G1211R*-genotype II were synthesized by Tsingke Biotech and cloned into the pUC57 vector. The plasmid p72-pPUR-TPA-ASFV-Fc carrying the *B646L gene* was preserved in our laboratory. The plasmid BPK2014-Cas12b was a kind gift from Wei Li. pY016 (pcDNA3.1-hLbCpf1) was a kind gift from Haoyi Wang. pC013-Twinstrep-SUMO-huLwaCas13a was purchased from Addgene (Catalog number: 90097). pC013-Twinstrep-SUMO-LbCas12a was constructed by replacing the LwaCas13a-encoding region in pC013-Twinstrep-SUMO-huLwaCas13a with the LbCas12a-encoding sequence.

The 5′-FAM-TTTTT-BHQ1-3′ probe used in the fluorescent reporter assay was synthesized by Sangon Biotech. The 5′-ROX-AUUUUUA-BHQ2-3′ probe for fluorescence readout and the 5′-FAM-AUUAUUAUUA-biotin-3′ and 5′-FAM-TTATTTTTTA-digoxin-3′ probes for lateral flow readout were ordered from Bio-lifesci (Guangzhou, China).

Sample processing

An extraction-free and ambient-temperature sample processing procedure is highly desirable for rapid on-site nucleic acid detection. Several studies have demonstrated that crude sample lysate can be directly used as input in isothermal nucleic acid amplification[96] and CRIPSPR-Dx assays.[55,68,69] Therefore, we incorporated a commercially available fast DNA extraction solution (Zhongdao Biotech, China) into our veterinary sample processing, following the manufacturer's protocol. This DNA extraction solution, originally designed for real-time PCR, functions at ambient temperature, making it suitable for our purposes.

Briefly, blood or swab samples were centrifuged at 8000 g/min for 2 mins. Five microliters of the supernatant was then mixed with 50 μL of solution A in a new tube and incubated at room temperature for 3 min. Finally, 50 μL of solution B was added to this mixture, vortexed thoroughly, and directly added to RPA or real-time PCR.

Nucleic acids of common swine pathogens were extracted using a TIANamp virus DNA/RNA kit (TIANGEN, China).

Conservation analysis of OBServe targeting sites

Twenty-seven non-redundant complete genomes of ASFV[52] were downloaded from the NCBI database on July 19th, 2021. Nucleotide sequences of each target gene were aligned using MEGA (version: 10.2.5) to determine highly conserved regions for designing RPA primers and guide RNAs (Figure S1).

Multiplex RPA of ASFV genes *B646L* and *MGF505-2R*

An RPA Nucleic Acid Amplification Kit (Qitian, China) was used for multiplex amplification. RPA primers were designed and screened according to the manufacturer's protocol. Multiplex RPA was performed using final concentrations of 62.5 nM *B646L* forward/reverse primers, 200 nM *MGF505-2R* forward/reverse primers, 25 μL rehydration buffer, 1 RPA pellet, 14 mM magnesium acetate and 15 μL DNA sample in a 50 μL reaction. Multiplex RPA reactions were performed at 39°C for 25 min. To increase amplification efficiency, we mixed the RPA reaction at 4 min and 10 min after initiation of the reaction.

Cas enzyme expression and purification

LwaCas13a and LbCas12a were expressed and purified according to the protocol from Feng Zhang[46] with some modifications. AapCas12b was expressed and purified according to the protocol from Wei Li.[54] For example, *Escherichia coli* Rosetta 2 (DE3) pLysS carrying plasmid pC013-Twinstrep-SUMO-huLwaCas13a was cultured using Luria broth with 100 μg/mL ampicillin at 37°C until the cells reached an optical density (OD, 600 nM) of 0.4-0.6. After cooling the flasks at 4°C for 30 min, we added 0.5 mM isopropyl-1-thio-b-D-galactopyranoside (IPTG, BBI, China) to induce expression and shook the cultures for 16 h at 220 r.p.m. in a prechilled 18°C biological shaker. The cells were harvested by spinning the culture down at 8000 × g for 5 min at 4°C. Cell pellets were lysed in lysis buffer (20 mM Tris-HCl, 500 mM NaCl, 1 mM DTT, pH 8.0) supplemented with protease inhibitors (cOmplete, EDTA-free, Roche, Swiss) and 2.5 unit/mL UltraNuclease (Yeasen Biotech, China) on ice. The lysate was cleared by centrifugation for 40 min at 4 °C at 12000 g. The cleared lysate was filtered using a 0.22 μm filter (Millipore, USA), followed by incubation with Step-Tactin XT 4Flow high capacity resin (IBA Life Science, Germany) in batch for 2 h by gentle shaking at 4°C. After washing with 15 column volumes of cold lysis buffer, the resin was resuspended in lysis buffer supplemented with 200 unit/mg SUMO Protease (Biomed, China) and 0.2% IGEPAL CA-630 (Sigma-Aldrich, USA) and incubated overnight at 4°C with rotation. Untagged Cas13a proteins were then diluted with cation exchange buffer (20 mM Tris-HCl, 1 mM DTT, 5% glycerol, pH 7.5), loaded onto an SP Sepharose fast flow (GE, USA) column and eluted by a NaCl salt gradient. The resulting fractions containing the protein were pooled and dialyzed using a 50 kDa dialyzer (Solarbio, China) overnight with storage buffer (20 mM Tris-HCl, 500 mM NaCl, 1 mM DTT,

10% glycerol, pH 8.0) at 4°C. Purified Cas13a proteins were concentrated using a 50 kDa Amicon Centrifugal Filter Unit (Millipore, USA), quantitated using the Bradford protein assay (Bio-Rad, USA), and stored at −80°C.

crRNA preparation

In vitro transcription was conducted using the T7 High RNA Transcription kit (Vazyme, China). In brief, a T7 promoter ssDNA forward primer and a conventional reverse primer were used to amplify the dsDNA template of crRNA, and the template was transcribed for 16 h at 37°C. Transcribed RNA was then treated with DNase I (Vazyme, China) for 15 min at 37°C and purified using VAHTS RNA Clean Beads (Vazyme, China). Detailed crRNA sequences used in this study are listed in Table S2.

Characterization of target dsDNA cleavage and collateral cleavage activity of AapCas12b and LwaCas13a

For the dsDNA target cleavage assay of AapCas12b, 1.2 μM AapCas12b protein, 1.2 μM sgRNA, 300 ng dsDNA substrate and 0.8 unit/μL Murine RNase Inhibitor (Vazyme, China) were incubated for 1 h at 60°C in cleavage buffer (NEBuffer 2.1, NEB, USA) as discribed.[54]

For the ssRNA target cleavage assay of LwaCas13a, 0.6 μM LwaCas13a protein, 0.6 μM crRNA, 1300 ng ssRNA substrate and 0.8 unit/μL Murine RNase Inhibitor were incubated for 1 h at 37°C in NEBuffer 1.1 as discribed.[97]

To test the orthogonal collateral cleavage of AapCas12b and LwaCas13a, 50 nM AapCas12b protein, 150 nM sgRNA, 10 nM dsDNA substrate, 0.8 unit/μL murine RNase inhibitor, 500 nM quenched ssDNA fluorescent probes and 500 nM quenched ssRNA fluorescent probes were incubated in NEBuffer 1.1 for 15 min at 60°C as discribed.[50] For LwaCas13a, an assay was performed with 50 nM LwaCas13a protein, 50 nM crRNA, 10 nM ssRNA substrate, 0.8 unit/μL murine RNase inhibitor, 500 nM quenched ssDNA fluorescent probes, 500 nM quenched ssRNA fluorescent probes and NEBuffer 1.1 for 15 min at 37°C as discribed.[50] The fluorescence signals of these reactions were recorded every minute by a LightCycler 96 (Roche, Swiss) in the FAM channel (for ssDNA probe) and ROX channel (for ssRNA probe). Detailed probe sequences are listed in Table S3.

Orthogonal CRISPR-Cas12/Cas13 detection assay

Previous studies report that the efficiency of Cas12a is suppressed by Cas13a assay components, leading to lower fluorescence[50] or a weaker test band on lateral flow strips for Cas12a detection compared with Cas13a.[44] To address this issue, we replaced the commonly used LbCas12a with a thermophilic Cas12 ortholog, AapCas12b, in the orthogonal CRISPR-Cas12/Cas13 system. In this modified design, the reaction temperature was initially set at 37°C for Cas13a detection, followed by a subsequent heating step to 60°C to inactivate Cas13a assay components[55] while maintaining higher efficiency for Cas12b.[56] This approach allows Cas13a and Cas12b to function independently at different stages of the reaction.

For side-by-side comparisons of the orthogonal CRISPR-Cas12a/Cas13a assay and orthogonal CRISPR-Cas12b/Cas13a assay, we performed orthogonal CRISPR-Cas12a/Cas13a assay with 60 nM Cas12a, 150 nM Cas12a-crRNA, 600 nM ssDNA probe, 50 nM Cas13a, 50 nM Cas13a-crRNA, 400 nM ssRNA probe, 0.5 unit/μL NxGenT7 RNA polymerase (Lucigen, USA), 1 mM rNTPs mix (Thermo Fisher Scientific, USA), 0.8 unit/μL Murine RNase Inhibitor, NEBuffer 1.1 and multiplex RPA product in a 50 μL reaction for 15 min at 37°C as discribed.[50]

An orthogonal CRISPR-Cas12b/Cas13a assay was modified from Tian et al.[50] by replacing LbCas12a with AapCas12b and used a two-step reaction scheme. Briefly, the orthogonal CRISPR-Cas12b/Cas13a assay was performed in 50 μL reaction volumes containing 50 nM Cas12b, 150 nM Cas12b-sgRNA, 600 nM ssDNA probe, 50 nM Cas13a, 50 nM Cas13a-crRNA, 400 nM ssRNA probe, 0.5 unit/μL NxGenT7 RNA polymerase, 0.25 mM rNTPs mix, 0.8 unit/μL Murine RNase Inhibitor, NEBuffer 1.1 and multiplex RPA product. This reaction was incubated for 5 min at 37°C, followed by 10 min at 60°C.

The fluorescence signals of these reactions were recorded every minute by a LightCycler 96 in the FAM channel (for ssDNA probe) and ROX channel (for ssRNA probe).

Detection via lateral flow strips

In this study, the readout was visualized using commercially available multiplexed lateral flow strips (HybriDetect 2T, Milenia, Germany) following the manufacturer's protocol. We generated the orthogonal CRISPR-Cas12b/Cas13a detection mix as described above, except replacing the fluorescent probes with biotinylated ssDNA probe at a final concentration of 1μM and digoxin-modified ssRNA probe at a final concentration of 150 nM. Detailed probe sequences are listed in Table S3.

After incubating the detection reaction for 15 minutes at 39°C, followed by 30 minutes at 60°C, the reaction was diluted 1:5 in DNase/RNase-Free water (TIANGEN, China). Subsequently, 10 μL of the diluted reaction mixture was directly loaded onto the sample pad area of the HybriDetect 2T lateral flow strips. The loaded strips were then placed into 80 μL of HybriDetect 2T Assay Buffer (Milenia, Germany) and incubated for 5 minutes at room temperature in an upright position. The lateral flow results were assessed by the user.

Real-time PCR of ASFV

Detection of ASFV was first performed using a commercially available single-plex real-time PCR kit targeting *B646L* (Zhongdao Biotech, China), followed by validation using a triplex real-time PCR kit (Lijian, China) for ASFV-positive samples.

Conventional PCR, Sanger sequencing and multiple sequence alignment

To determine the genotype of ASFV veterinary samples, we amplified the 3′ end of *B646L* using a conventional PCR method[62] and sequenced it using Sanger sequencing (Sangon Biotech, China). Fourteen nucleotide sequences of veterinary samples and 10 reference ASFV *B646L* genes were aligned using MAGA (version: 10.2.5), and a maximum likelihood phylogenetic tree was generated based on this alignment.

QUANTIFICATION AND STATISTICAL ANALYSIS

Fluorescence values were reported as background-subtracted, with the fluorescence value collected at the beginning subtracted from the final fluorescence value. Data were visualized using GraphPad Prism 7, and the results are expressed as the mean ± SEM (standard error of the mean). Significant differences between two groups were determined by unpaired Student's *t*-test (two tail). Asterisks denote the level of statistical significance: *, $p \leq 0.05$; **, $p \leq 0.01$; ***, $p \leq 0.001$.